J|A|C|S
ARTICLES
Published on Web 11/28/2002

Kinetics of Reductive N−O Bond Fragmentation: The Role of a Conical Intersection

Edward D. Lorance, Wolfgang H. Kramer, and Ian R. Gould*

Contribution from the Department of Chemistry and Biochemistry, Arizona State University, Box 871604, Tempe, Arizona 85287-1604

Received June 3, 2002. Revised Manuscript Received September 13, 2002

Abstract: *N*-alkoxyheterocycles can act as powerful one-electron acceptors in photochemical electron-transfer reactions. One-electron reduction of these species results in formation of a radical that undergoes N−O bond fragmentation to form an alkoxy radical and a neutral heterocycle. The kinetics of this N−O bond fragmentation reaction have been determined for a series of radicals with varying substituents and extents of delocalization. Rate constants varying over 7 orders of magnitude are obtained. A reaction potential energy surface is described that involves avoidance of a conical intersection. A molecular basis for the variation of the reaction rate constant with radical structure is given in terms of the relationship between the energies of the important molecular orbitals and the reaction potential energy surface. Ab initio and density functional electronic structure calculations provide support for the proposed reaction energy surface.

Introduction

Studies of single-electron transfer-initiated bond fragmentation reactions have been an important theme in physical organic chemistry in recent years.[1] Kinetic studies of both radical anions formed upon reduction and radical cations formed upon oxidation have resulted in the development of several new and important mechanistic principles.[1] Photoinduced single-electron-transfer-induced bond fragmentation reactions also find many practical applications, particularly in the area of imaging technology.[2] For example, fragmentation of a radical cation results in the formation of a radical ($Y^{\bullet}$) and an electrophile (X^+), eq 1a. If X^+ is a proton, H^+, then eq 1 forms the basis of a photoacid system.[3] Correspondingly, fragmentation of a radical anion can form a radical ($Y^{\bullet}$) and a nucleophile or base, (X^-), eq 1b. The radicals formed in such processes have been used in photoinitiated polymerization systems.[2]

$$X{-}Y \xrightarrow{-e^-} X{-}Y^{\bullet +} \rightarrow X^+ \; Y^{\bullet} \qquad (1a)$$

$$X{-}Y \xrightarrow{+e^-} X{-}Y^{\bullet -} \rightarrow X^- \; Y^{\bullet} \qquad (1b)$$

The energetics of photoinduced single-electron-transfer reactions, ΔG_{et}, are usually described in terms of the appropriate redox potentials and the energy of the excited state. For the case of photochemical reduction of a fragmentable X−Y molecule using an excited-state electron donor sensitizer molecule, S*, eq 2a, ΔG_{et} is given by eq 2b.[4] Here, E_{ex}^{S*} is the energy of the excited-state sensitizer, E_{ox}^{S} is the oxidation potential of the sensitizer, and E_{red}^{X-Y} is the reduction potential of the X−Y molecule.

$$S^* + X{-}Y \rightarrow S^{\bullet +} + X{-}Y^{\bullet -} \qquad (2a)$$

$$\Delta G_{et} = (E_{ox}^{S} + E_{red}^{X-Y}) - E_{ex}^{S*} + C \qquad (2b)$$

C is a term that corrects for Coulombic interactions in the product geminate pair and is often negligible in polar solvents.[4] To be broadly useful in technological applications, photochemically induced fragmentation of an X−Y molecule should occur with as wide a range of excitation wavelengths as possible, that is, the reaction should proceed with as small a sensitizer excitation energy E_{ex}^{S*} as possible.[5] For the example given in eq 2b, this means that the X−Y molecule should be easy to reduce (E_{red}^{X-Y} should be as small a negative number as possible). One obvious way to achieve facile reduction is to use a positively charged X−Y molecule (or a negatively charged molecule in a corresponding oxidation reaction). Indeed, the two technological applications of photoinduced bond fragmentation that have been demonstrated over the widest range of excitation wavelengths use this approach. Photochemical oxidation of borate salts has been studied extensively by Schuster et al.[5b,6] One-electron oxidation of an alkyltriarylborate ($^-BRAr_3$) results in formation of a boranyl radical, $^{\bullet}BRAr_3$, which

* To whom correspondence should be addressed. E-mail: igould@asu.edu.

(1) (a) Baciocchi, E.; Bietti, M.; Lanzalunga, O. *Acc. Chem. Res.* **2000**, *33*, 243. (b) Gaillard, E. R.; Whitten, D. G. *Acc. Chem. Res.* **1996**, *29*, 292. (c) Albini, A.; Fasani, E.; Freccero, M. *Adv. Electron Transfer Chem.* **1996**, *5*, 103. (d) Saveant, J.-M. *Adv. Electron Transfer Chem.* **1994**, *4*, 53. (e) Maslak, P. *Top. Curr. Chem.* **1993**, *168*, 1. (f) Popielarz, R.; Arnold, D. R. *J. Am. Chem. Soc.* **1990**, *112*, 3068. (g) Dinnocenzo, J. P.; Farid, S.; Goodman, J. L.; Gould, I. R.; Todd, W. P.; Mattes, S. L. *J. Am. Chem. Soc.* **1989**, *111*, 8973. (h) Mattes, S. L.; Farid, S. *Org. Photochem.* **1983**, *6*, 233.

(2) See, for example: (a) Paczkowski, J.; Neckers, D. C. In *Electron Transfer in Chemistry;* Balzani, V., Ed.; Wiley-VCH: New York, 2001; Vol. 5, p 516. (b) Reiser, A. *Photoreactive Polymers, the Science and Technology of Resists*; Wiley: New York, 1989.

(3) See, for example: (a) Saeva, F. D. *Adv. Electron Transfer Chem.* **1994**, *4*, 1. (b) DeVoe, R. J.; Olofson, P. M.; Sahyun, M. R. V. *Adv. Photochem.* **1992**, *17*, 313. (c) Crivello, J. V. *Adv. Polym. Sci.* **1984**, *62*, 1.

(4) Weller, A. *Z. Phys. Chem. (Munich)* **1982**, *130*, 129.

(5) (a) Gould, I. R.; Shukla, D.; Giesen, D.; Farid, S. *Helv. Chim. Acta*, **2001**, *84*, 2796. (b) Chatterjee, S.; Gottschalk, P.; Davis, P. D.; Schuster, G. B. *J. Am. Chem. Soc.* **1988**, *110*, 2326.

(6) Schuster, G. B. *Adv. Electron Transfer Chem.* **1991**, *1*, 163.

Scheme 1

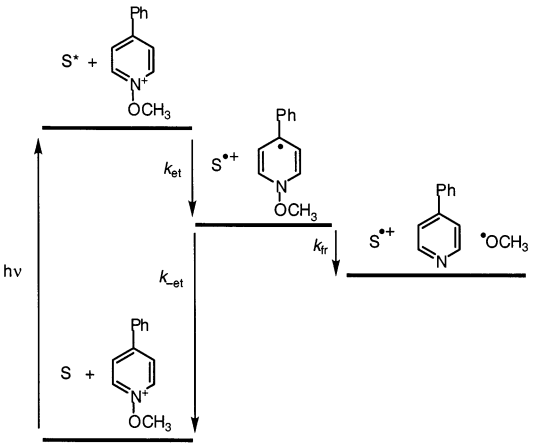

efficiently fragments to an alkyl radical and a triarylborane, eq 3. Alkyl radicals generated this way using visible light sensitization have been used to initiate radical polymerization reactions in a commercial technological application.[7]

$$^{-}BRAr_3 \xrightarrow{-e^-} {}^{\bullet}BRAr_3 \rightarrow R^{\bullet} + BAr_3 \qquad (3)$$

The radical initiation system that has been demonstrated with the widest range of wavelengths involves reduction of an *N*-methoxypyridinium compound, Scheme 1.[5a,8,9] Exothermic electron transfer, k_{et}, from an excited sensitizer results in formation of the sensitizer radical cation, $S^{\bullet+}$, and a pyridyl radical. Fragmentation of the pyridyl radical, k_{fr}, produces a methoxy radical that initiates radical polymerization reactions.[5a,8] Sensitizers with absorption maxima even greater than 750 nm have been shown to be useful in this process.[5a] The reactions proceed with reasonable photon efficiency, which means that fragmentation of the pyridyl radical is rapid enough to compete favorably with the energy-wasting return electron transfer process in the geminate pair (k_{-et}, Scheme 1).[5a] In general, identification of large values for k_{fr} is a common goal in studies of photoinduced fragmentation reactions.[1] For technological applications, large values of k_{fr} are essential for high photon efficiency.[5]

Although facile reduction of X−Y is beneficial so that the energy of the excited state can be as low as possible (eq 2b), the thermodynamic favorability of bond fragmentation decreases with increasing ease of reduction of X−Y. For the case of reduction of a positively charged molecule ($X-Y^+$) to a radical ($X-Y^{\bullet}$) that undergoes fragmentation, the thermodynamic cycle of Scheme 2 can be given.[5a,10] Scheme 2 shows that the bond dissociation energy for the radical $X-Y^{\bullet}$, BDE ($X-Y^{\bullet}$), will increase (i.e., fragmentation will become less favorable) as the reduction potential of the $X-Y^+$ molecule (E_{red}^{X-Y+}) becomes less negative, that is, as $X-Y^+$ becomes easier to reduce. Purely the basis of on thermodynamic arguments, the radical derived

Scheme 2

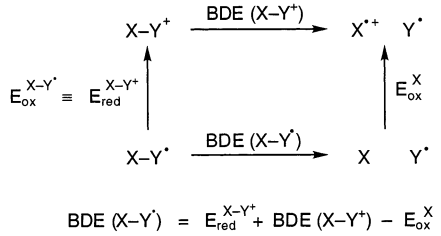

from an $X-Y^+$ compound that is easier to reduce may have a smaller value of k_{fr}.

One obvious question therefore relates to the extent to which the kinetics of bond fragmentation in species such as $X-Y^{\bullet}$ in Scheme 2 actually vary with the reduction potential of the precursor $X-Y^+$ and what other factors influence the rates of these reactions. In the literature, the rate constants for cleavage of two radicals formed upon reduction of *N*-alkoxyheterocycles have been reported, eq 4.[11] Both can be considered to be cleavage reactions of *N*-alkoxypyridyl radicals with electron-withdrawing substituents, *p*-(*N*-ethoxypyridyl) in 4a[11a] and *p*-cyano in 4b.[11b] As such, both radical precursors are relatively easy to reduce and might be considered to be equally useful with a wide range of sensitizers. However, the rate constants of the two radical cleavage reactions differ by an astonishing 6 orders of magnitude, eq 4.

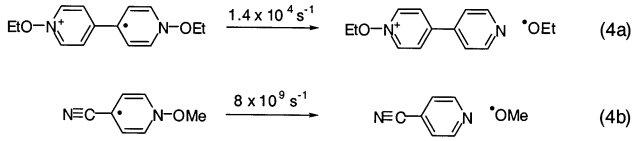

The fragmentation reaction in 4b occurs with such a sufficiently high rate constant that it would be expected to compete usefully with return electron transfer in a sensitization process such as that illustrated in Scheme 1. The reaction in eq 4a is sufficiently slow to be essentially useless in such a reaction scheme. Obviously, the "substituent" in eq 4a is a somewhat stronger withdrawing group than that in eq 4b, and reduction of the pyridinium precursor in the latter case will thus be somewhat more difficult than in the former. According to the thermodynamic arguments given above, it is understandable that the reaction in eq 4a is slower than that in eq 4b. However, it is also clear that the radical in eq 4a is more delocalized and resonance stabilized than that in eq 4b. The relative importance of these and other possible factors in determining the very large difference in k_{fr} values in this case is not clear.

To determine the factors that control the rate constants for fragmentation in such radicals, the relative importance of electron-withdrawing and delocalizing substituents needs to be further explored. Here we describe an extensive study of the kinetics of fragmentation of a series of *N*-methoxyheterocyclic radicals, with varying substituents and extents of delocalization. One goal of this work is to identify single-electron-transfer-induced fragmentation reactions that occur with very high rate constants, for the reasons discussed above. A further goal is to develop a detailed description of the factors that control the rate constants for fragmentation in radicals such as these and

(7) Rastogi, A. K.; Wright, R. F. *Proc. SPIE-Int. Soc. Opt. Eng.* **1989**, *1079*, 183.
(8) Farid, S. Y.; Haley, N. F.; Moody, R. E.; Specht, D. P. U.S. Patents 4,743,528, 4,743,529, 4,743,530, and 4,743,531, 1988.
(9) (a) Schnabel, W. *Macromol. Rapid Commun.* **2000**, *21*, 628. (b) Zhu, Q. Q.; Schnabel, W. *Eur. Polym. J.* **1997**, *3*, 1325. (c) Yagci, Y.; Schnabel, W. *Macromol. Symp.* **1994**, *85*, 115. (d) Kayaman, N.; Onen, A.; Yagci, Y.; Schnabel, W. *Polym. Bull. (Berlin)* **1994**, *32*, 589.
(10) (a) Popielarz, R.; Arnold, D. R. *J. Am. Chem. Soc.* **1990**, *112*, 3068. (b) Maslak, P.; Vallombroso, T. M.; Chapman, W. H., Jr.; Narvaez, J. N. *Angew. Chem., Int. Ed. Engl.* **1994**, *33*, 73.
(11) (a) Wolfle, I.; Lodaya, J.; Sauerwein, B.; Schuster, G. B. *J. Am. Chem. Soc.* **1992**, *114*, 9304. (b) Bockman, T. M.; Lee, K. Y.; Kochi, J. K. *J. Chem. Soc., Perkin Trans. 2* **1992**, *9*, 1581.

Scheme 3

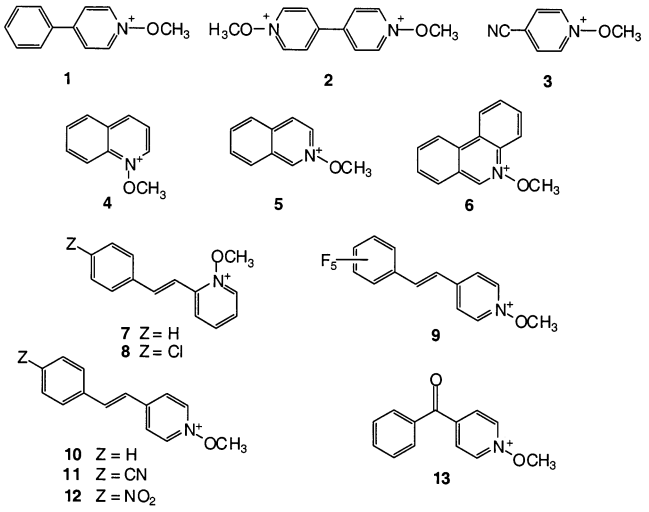

Scheme 4

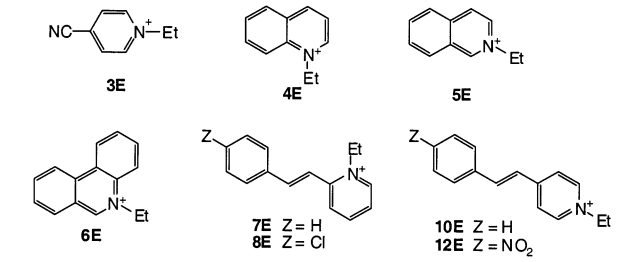

other one-electron-reduced species. Specifically, a molecular basis is sought for the relative rate effects predicted by thermodynamic cycles such as those in Scheme 2. A description of the radical reactions that involves the avoidance of a conical intersection is given.[12] A relationship between the energies of the important molecular orbitals and the reaction potential energy surface is described that is supported by density functional electronic structure calculations.

Results and Discussion

Molecular Structures. The structures summarized in Scheme 3 have been investigated. Structures **1**, **4**−**7**, and **10** exhibit differing degrees of delocalization. Structure **3** has a simple electron-withdrawing group (ignoring the delocalization in the cyano group), and **2**, **8**, **9**, **11**−**13** include both delocalizing and electron-withdrawing effects.

The *N*-ethyl-substituted heterocycles summarized in Scheme 4 were also used in the kinetic measurements, see further below.

Kinetic Measurements. Two methods were used to measure the rate constants of fragmentation of the radicals. For those with rate constants smaller than ca. 1×10^8 s^{-1}, the radicals were generated in diffusive second-order reduction reactions, and the decay of the radicals was observed directly as a function of time in a conventional nanosecond transient absorption experiment.

For compound **12**, the radical was generated using the DCA/biphenyl cosensitization system in acetonitrile solvent, Scheme 5.[13a] Excitation of 9,10-dicyanoanthracene (DCA) in the presence of ca. 1 M biphenyl (BP) results in electron-transfer quenching and efficient formation within ca. 5 ns of the DCA radical anion ($DCA^{\bullet-}$) and the biphenyl radical cation ($BP^{\bullet+}$) in solution.[13a] In the presence of ca. 10^{-2} M **12** and 10^{-2} M benzyltrimethylsilane (BTS), within another ca. 10 ns, the $DCA^{\bullet-}$ reduces **12** to the corresponding radical, and the $BP^{\bullet+}$ oxidizes the BTS to its radical cation ($BTS^{\bullet+}$). Within a few nanoseconds of its formation, the $BTS^{\bullet+}$ fragments to form a benzyl radical ($Bz^{\bullet}$), which absorbs only in the UV region.[1g] Thus, within ca. 15 ns of the laser pulse, the only visible absorbing transient species should be the radical derived from **12**. Under these conditions, a transient species is observed with an absorption maximum at ca. 575 nm. This transient is assigned to the radical on the basis of the fact that it is formed at the same rate at which the $DCA^{\bullet-}$ decays and that a very similar absorption is observed with the corresponding *N*-ethyl compound **12E**. Importantly, the absorption from **12E** is relatively long-lived (the first half-life is greater than 10 μs) and decays by a mixture of first- and second-order processes, whereas that from **12** decays in a rapid first-order process, consistent with N−O bond cleavage. Measurements as a function of temperature in acetonitrile allow a room-temperature rate constant for fragmentation of 1.0×10^8 s^{-1} to be determined (Table 1).

Scheme 5

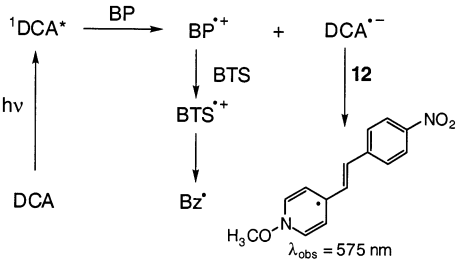

Table 1. Arrhenius Activation Parameters for Fragmentation of Radicals Formed by Reduction of *N*-Methoxyheterocycles[a]

Structure	Number	k_{fr}, s^{-1}	E_a, kcal mol^{-1}	Log A, s^{-1}
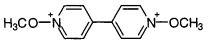	**2**	4.0×10^{4} [b]	10.5 [b]	12.2 [b]
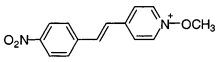	**12**	1.0×10^{8} [c]	7.0 [c]	13.2 [c]

[a] See Experimental Section for estimates of errors. [b] In 1,2-dichloroethane solvent. [c] In acetonitrile solvent.

For compound **2**, electron transfer from the 9-thioxanthenone triplet was used to generate the reduced form, in a manner similar to that previously reported for the corresponding diethoxy compound.[11a] For both **2** and **12**, experiments were performed as a function of temperature (Table 1).

For the radicals that fragmented faster than ca. 1×10^8 s^{-1}, diffusive reduction could not be used since the rates of formation of the reactive radicals would in most cases be slower than the rates of their fragmentations. In these cases, a method involving excitation of a charge-transfer complex was used to determine the fragmentation rate constants.[11b,14] Excitation of a suitable CT complex forms a geminate pair containing the reactive radical. The rate constant for fragmentation can be extracted

(12) (a) Yarkony, D. A. *Acc. Chem. Res.* **1998**, *31*, 511. (b) Yarkony, D. R. *J. Phys. Chem.* **2001**, *105*, 6277.
(13) (a) Gould, I. R.; Ege, D.; Moser, J. E.; Farid, S. *J. Am. Chem. Soc.* **1990**, *112*, 4290. (b) Lewis, F. D.; Dykstra, R. E.; Elbert, J. E.; Gould, I. R.; Farid, S. *J. Am. Chem. Soc.* **1990**, *112*, 8055.
(14) (a) Bockman, T. M.; Hubig, S. M.; Kochi, J. K. *J. Am. Chem. Soc.* **1998**, *120*, 6542. (b) Bockman, T. M.; Hubig, S. M.; Kochi, J. K. *J. Org. Chem.* **1997**, *62*, 2210.

Scheme 6

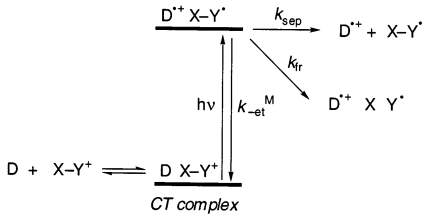

from the overall dynamics of the geminate pair. The method used here is similar to one described previously by Kochi et al.,[11b,14] except that an additional process of the geminate pair is included in the kinetic analysis, that is, diffusive separation of the partners. This method has not been described previously and thus is discussed in some detail here.

The *N*-methoxy- and *N*-ethyl-substituted compounds of Schemes 3 and 4, $X-Y^+$, are generally strong one-electron acceptors. Addition of a suitable electron donor compound, D, to an $X-Y^+$ solution results in reversible formation of a charge-transfer (CT) complex (D $X-Y^+$, Scheme 6), characterized by a broad CT electronic absorption tailing into the visible region.[11b,14,15] Excitation into this CT absorption band results in formation of the first excited state of the CT complex, that is, a geminate radical cation/radical pair ($D^{\bullet+}$ $X-Y^{\bullet}$, Scheme 6). The geminate pair can undergo three processes, that is, return electron transfer to regenerate the ground-state complex (D $X-Y^+$, k_{-et}^M),[15b] separation to form a separated radical cation and radical ($D^{\bullet+}$ + $X-Y^{\bullet}$, k_{sep}),[15c] and fragmentation of the N−O bond to form a methoxy radical and the neutral heterocycle (X $Y^{\bullet}$, k_{fr}). The $X-Y^{\bullet}$ pair that separates will also fragment, but this reaction is not observed in the geminate pair.

The donor D is chosen so that the time scale for return electron transfer is as similar to that of fragmentation as possible. Accurate extraction of k_{-et} and k_{fr} from the measured rate constant for decay of the geminate pair is only possible when these two processes are competitive (see further below). With the exception of two cases described separately below, three donors have been used for all of the experiments, that is, *p*-trianisyamine (TAA), stilbene (S), and biphenyl (BP). Return electron transfer occurs in the Marcus inverted region for the systems studied here,[13] and k_{-et} increases with decreasing oxidation potential of the donor.[13] The oxidation potential decreases in the order BP to S to TAA.[13] Hence, the slower fragmenting radicals were generally measured using BP as the donor, and the fastest was measured using TAA.

The donor D is also chosen so that $D^{\bullet+}$ has a characteristic and strong electronic absorption band in the visible region. The decay kinetics of the geminate pair can then be monitored via the absorptions of $D^{\bullet+}$. The absorption of $D^{\bullet+}$ initially decays due to return electron transfer and reaches a persistent value (on the picosecond time scale) that corresponds to the number of the geminate pairs that either separate or undergo fragmentation. Typical data are illustrated in Figures 1 and 2, for excitation of the CT complexes formed between *N*-methoxyphenanthridinium tetrafluoroborate, **6** (Figure 1), *N*-methoxy-2-styrylpyridinium tetrafluoroborate, **7** and *N*-ethyl-2-styrylpyridinium hexafluorophosphate, **7E** (Figure 2), as acceptors, and stilbene as the donor, in butyronitrile at room temperature. The spectra in Figure 1 are of the geminate stilbene radical cation/phenanthridyl radical geminate pair. It is well-known that the absorption spectra of such geminate pairs can be very well described as the sum of the absorptions of the two partners (see, for example, refs 14 and 15b,c and refs therein), in this case the stilbene radical cation and the phenanthridyl radical. The

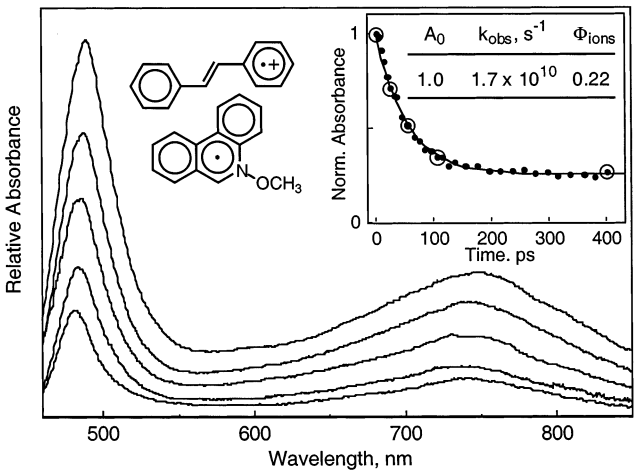

Figure 1. Relative absorbance spectra (arbitrary absolute units) observed for excitation of the charge-transfer complex formed between *N*-methoxyphenanthridinium tetrafluoroborate (**6**) and stilbene in butyronitrile at room temperature, showing decay of the geminate pair due to return electron transfer. The spectra were taken at ca. 0, 25, 50, 100, and 400 ps after the excitation pulse. (Inset) Decay of the absorbance integral from 482 to 491 nm as a function of time ($A(t)$, filled circles). The larger open circles represent the times at which the spectra were acquired. The smooth line through the data shows the best fit to eq 9, using the parameters shown.

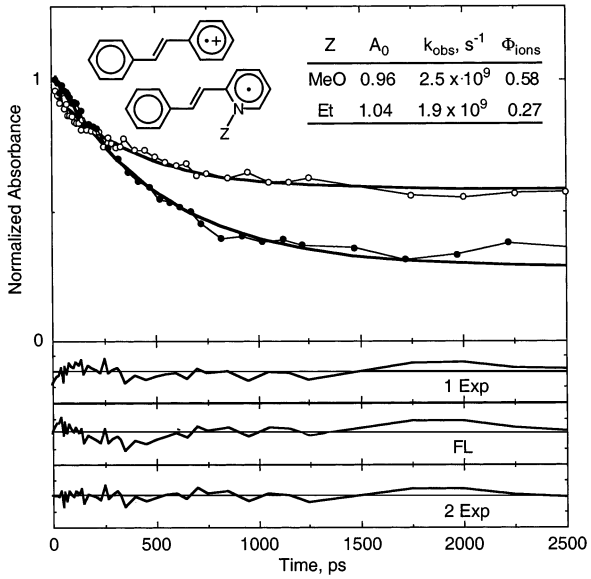

Figure 2. (Top panel) Normalized absorbance decays as a function of time, $A(t)$, for geminate pairs of *N*-methoxy-2-styrylpyridyl (open circles) and *N*-ethyl-2-styrylpyridyl radicals (closed circles) with stilbene as the donor in butyronitrile at room temperature. The curves through the data represent best fits to eq 9 with the parameters shown. The three lower panels show residual plots for fits of the *N*-methoxy radical data to (1 Exp) single-exponential kinetics using eq 9 with the parameters shown, (FL) the Fick's law diffusion model of eq 11 with 1.87, 18.78, and 303 for κ, λ, and τ, respectively, and (2 Exp) double-exponential kinetics, eq 12, with 0.11, 1.67×10^{10} s^{-1}, 0.32, 1.76×10^9 s^{-1} and 0.57 for A_F', k_F', A_S', k_S' and Φ_{ions}, respectively.

(15) (a) Mulliken, R. S.; Pearson, W. B. *Molecular Complexes: A Lecture and Reprint Volume*; Wiley: New York, 1966. (b) Arnold, B. R.; Noukakis, D.; Farid, S.; Goodman, J. L.; Gould, I. R. *J. Am. Chem. Soc.* **1995**, *117*, 4399. (c) Arnold, B. R.; Farid, S.; Goodman, J. L.; Gould, I. R. *J. Am. Chem. Soc.* **1996**, *118*, 5482.

extinction coefficient of the stilbene radical cation in the visible region is very large,[13b] and indeed the spectra in Figure 1 are essentially identical to the reported spectrum of the stilbene radical cation.[13b] We conclude that the phenanthridyl radical absorbance is sufficiently small so that it cannot be observed in the presence of the stilbene radical cation. Indeed, for all of the CT complexes studied with all three donors, the absorption spectra of the geminate pairs were essentially those of the radical cations, with absorption maxima at ca. 670 nm (for $BP^{\bullet+}$),[13a] ca. 475 nm (for $S^{\bullet+}$),[13b] and ca. 710 nm (for $TAA^{\bullet+}$).[13a]

The observed rate constant for exponential decay of the absorption signal to the persistent level, $k_{obs}{}^{M}$, is equal to the sum of the rate constants for all of the competing processes, eq 5a. The ratio of the persistent signal to that at time zero can be termed the quantum yield for formation of separated radicals and radical ions, $\Phi_{ions}{}^{M}$. As shown in eq 5b, $\Phi_{ions}{}^{M}$ is equal to the ratio of the sum of the rate constants that do not decrease the radical cation signal to the sum of all rate constants, eq 5b.

$$k_{obs}{}^{M} = k_{-et}{}^{M} + k_{sep} + k_{fr} \tag{5a}$$

$$\Phi_{ions}{}^{M} = \frac{k_{sep} + k_{fr}}{k_{-et}{}^{M} + k_{sep} + k_{fr}} \tag{5b}$$

There is not enough information in the two pieces of experimental data, $k_{obs}{}^{M}$ and $\Phi_{ions}{}^{M}$, to determine values for all three elementary rate constants. The rate constant for diffusive separation, k_{sep}, was thus determined independently from studies of the corresponding nonfragmenting *N*-ethylheterocyclic compounds (Scheme 4) in otherwise identical charge-transfer complexes. The rate constant for decay of the geminate pairs in this case, $k_{obs}{}^{E}$, is given by eq 6a, and the corresponding quantum yield for formation of separated radicals, $\Phi_{ions}{}^{E}$, by eq 6b.

$$k_{obs}{}^{E} = k_{-et}{}^{E} + k_{sep} \tag{6a}$$

$$\Phi_{ions}{}^{E} = \frac{k_{sep}}{k_{-et}{}^{E} + k_{sep}} \tag{6b}$$

The rate constants for return electron transfer and separation in these geminate pairs, $k_{-et}{}^{E}$ and k_{sep} respectively, are obtained directly using eqs 7a, b.

$$k_{sep} = \Phi_{ions}{}^{E} \cdot k_{obs}{}^{E} \tag{7a}$$

$$k_{-et}{}^{E} = k_{obs}{}^{E} - k_{sep} \tag{7b}$$

Since differences in mass and shape of the *N*-methoxy- and *N*-ethyl-substituted compounds are very small, k_{sep} can safely be assumed to be the same for the geminate pairs for both types of compound. Values for k_{fr} and $k_{-et}{}^{M}$ are thus obtained using eqs 8a, b.

$$k_{fr} = \Phi_{ions}{}^{M} \cdot k_{obs}{}^{M} - k_{sep} \tag{8a}$$

$$k_{-et}{}^{M} = k_{obs}{}^{M} - k_{sep} - k_{fr} \tag{8a}$$

Typical kinetic data are shown in Figures 1 and 2. The absorbance of the normalized stilbene radical cation in each geminate pair, $A(t)$, is shown as a function of time, t, together with exponential fits to the data according to eq 9, where, A_0 is the absorbance at zero time.

$$A(t) = (A_0 - \Phi_{ions})\, e^{-k_{obs} \cdot t} + \Phi_{ions} \tag{9}$$

As discussed above, in most cases, the absorbances of the $X-Y^{\bullet}$ radicals were too small compared to that of the $D^{\bullet+}$ ion to be directly observed in these experiments. However, for several of the styryl-substituted pyridiniums the $X-Y^{\bullet}$ absorbances were sufficiently large to be observed. For compounds **9** and **11**, a somewhat different method for obtaining k_{fr} was used that takes advantage of this fact. For these acceptors, CT complexes were studied with 1,2,4-trimethylbenzene (TMB) as the donor. Unlike the other donors, the $TMB^{\bullet+}$ has comparatively weak absorptions in the visible region,[13a] which allowed the absorptions due to reduced **9** and **11** to be observed at ca. 440 and 470 nm, respectively. The $X-Y^{\bullet}$ absorbances decay via biexponential kinetics. A faster decay is observed due to the radicals in the geminate pairs, followed by a slower decay due to fragmentation of the radicals that escape the geminate pair. The decay kinetics are described by eq 10, where A_F, k_f and A_S, k_f refer to the amplitudes and observed rate constants associated with the faster and slower exponential components, respectively. At wavelengths where only the radical $X-Y^{\bullet}$ is observed and not the $D^{\bullet+}$, no persistent signal is observed, since all of the radicals decay either by return electron transfer within the geminate pair or by fragmentation after separation.

$$A(t) = A_F\, e^{-k_F \cdot t} + A_S\, e^{-k_S \cdot t} \tag{10a}$$

$$k_{fr} = k_S \tag{10b}$$

Under these conditions, the slow observed rate, k_S, is simply the rate constant for fragmentation of the separated radicals, k_{fr}. The fast observed rate, k_F, is equal to the sum of the competing rates as described above, $k_{obs}{}^{M}$, assuming that fragmentation occurs with the same rate constant both in the geminate pair and when separated. Values for $(k_{-et}{}^{M} + k_{sep})$ are obtained by subtracting k_{fr} from k_F.

A possible kinetic complication that has been considered in other studies of geminate kinetics is that the return electron transfer rate may vary with separation distance.[16] To test this possibility, we attempted to fit the kinetic data using Shin and Kapral's equation for the time-dependent probability of geminate pair survival, developed using Fick's diffusion law and the radiation boundary condition, eq 11.[16]

$$P(\tau) = 1 - \frac{\lambda}{\kappa(1+\lambda)} \left\{ \operatorname{erfc}\left[\frac{\kappa - 1}{2\sqrt{\tau}}\right] - e^{[(1+\lambda)(\kappa-1)]} e^{[(1+\lambda)^2 \tau]} \operatorname{erfc}\left[(1+\lambda)\sqrt{\tau} + \frac{\kappa - 1}{2\sqrt{\tau}}\right] \right\} \tag{11}$$

Here, τ is the ratio between elapsed time and the diffusive time constant τ_0 ($\tau_0 = \sigma^2/D_c$, where σ is the sum of the hard-sphere collision radii and D_c is the mutual diffusion coefficient). The parameter κ is the ratio between the initial pair separation and the sum of the hard-sphere collision radii, λ is the ratio between

(16) (a) Shin, K. J.; Kapral, R. *J. Chem. Phys.* **1978**, *69*, 3685. (b) Scott, T. W.; Liu, S. N. *J. Phys. Chem.* **1989**, *93*, 1393. (c) Hyde, M. G.; Beddard, G. S. *Chem. Phys.* **1991**, *151*, 239.

Scheme 7

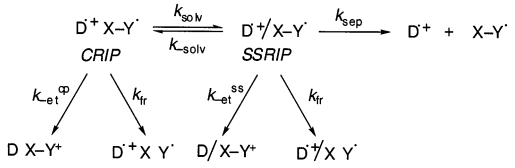

the effective rate constant for reactions that decrease $D^{\bullet+}$ to the rate constant for diffusional separation, and erfc is the complimentary error function.

Inspection of the residuals corresponding to the best fit to the data for the *N*-methoxy-2-styrylpyridinium (**7**) using this method, Figure 2, reveals that eq 11 is actually a poorer description of the kinetic behavior than the simple exponential description. Similar results were obtained for the other CT complexes studied here (data not shown). For this reason and the fact that extraction of elementary rate constants from κ and λ is not possible without further assumptions,[16b,c] we chose not to use the kinetic approach of eq 11.

A perhaps more sophisticated approach to the problem of variation of return electron transfer rate with distance, which takes into account accepted radical distribution functions for particles in condensed media,[17] includes two possible geminate species, that is, contact and solvent-separated radical ion pairs, CRIP and SSRIP, respectively, Scheme 7.[18] Return electron transfer in a contact pair, k_{-et}^{cp}, may be larger than in a solvent-separated pair, k_{-et}^{ss}, because of larger electronic coupling.[18] Formation of the SSRIP from the CRIP is understood as a solvation process, k_{solv}, and overall separation occurs from the SSRIP, that is, the meaning of k_{sep} is somewhat different from that in Scheme 6.[15b,18] A complete description also includes the fact that the SSRIP and CRIP may interconvert via k_{-solv}.[18] For this kinetic scheme, double exponential kinetics should be observed for the absorption decays of the geminate species, eq 12.

$$A(t) = A_F' \, e^{-k_F' \cdot t} + A_S' \, e^{-k_S \cdot t} + \Phi_{ions} \qquad (12)$$

For such a kinetic analysis to be useful, however, neither of the amplitudes A_F' or A_S' should be much larger than the other, and the values of k_F' and k_S' should not be too similar.[18c] In other words, the lifetimes of both geminate pairs should be both measurable and different. In turn this means that the CRIP should not solvate to form the SSRIP so rapidly that the former pair is not observed, and the SSRIP should be sufficiently long-lived that a reasonable population builds up during the time scale of the experiment. The lifetime of the SSRIP depends on the relative values of k_{-et}^{ss}, k_{fr}, k_{sep}, and k_{-solv} in a complex manner. Clearly, kinetic data that can be fitted reasonably well using a single-exponential function must be fitted as well or even better by using a double exponential function. Inspection of the residuals corresponding to the best fit to the data for the *N*-methoxy-2-styrylpyridinium (**7**), Figure 2, reveals a slightly better fit for the double compared to that of the single-exponential analysis (based on the sum of the squares of the residuals), as expected. However, the correlation coefficients are barely different for the *N*-methoxy compound, 0.9566 and 0.9552 for single and double exponential analyses, respectively. Furthermore, a two-tailed *z*-test using Fischer's *Z* transformation for determining the significance of a difference between two correlation coefficients demonstrates that the double-exponential analysis is not statistically different from the single-exponential analysis, up to and beyond the 99% confidence limit.[19] Double-exponential analyses of other geminate pairs (data not shown) provided even less satisfactory results. Either one of the preexponential factors A_F' or A_S' was very small, or k_F' and k_S' were very similar, implying that the decay kinetics were equally well described by single-exponential kinetics. Presumably, one of the two geminate pairs is being observed mainly in these experiments because the lifetime of the other is too short to be readily detected. For this reason, the single-exponential analysis method for analyzing the data described above was used. It is difficult to say whether the observed fragmentation occurs in the CRIP or the SSRIP, although this is not important for the present purposes.

Table 2. Rate Constants for Fragmentation, Return Electron Transfer, and Separation, for Geminate Pairs of Reduced *N*-Methoxyheterocycles at Room Temperature[a]

Structure	Number	k_{fr}, s^{-1}	k_{-et}, s^{-1}	k_{sep}, s^{-1} [b]
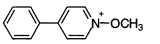	**1**	2.7×10^{11} [c]	1.5×10^{12} [c]	d
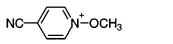	**3**	1.2×10^{10} [e]	2.2×10^{10} [e]	2.9×10^{9} [e]
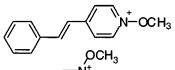	**10**	4.6×10^{9}	6.3×10^{9}	5.7×10^{8}
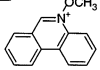	**6**	3.1×10^{9}	1.4×10^{10}	5.6×10^{8}
	**4**	2.0×10^{9}	2.3×10^{10}	9.2×10^{8}
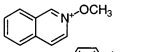	**5**	1.5×10^{9}	2.6×10^{10}	8.2×10^{8}
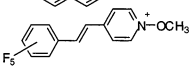	**9**	1.1×10^{9} [f]	3.0×10^{10} [f,g]	
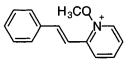	**7**	1.0×10^{9}	9.8×10^{8}	5.2×10^{8}
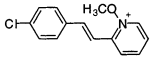	**8**	1.0×10^{9}	1.3×10^{9}	5.5×10^{8}
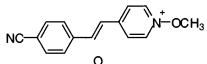	**11**	7.5×10^{8}	3.0×10^{10} [f,g]	
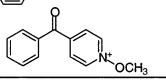	**13**	2.8×10^{8}	4.7×10^{10}	5.7×10^{8} [h]

[a] For charge-transfer complexes of the radical precursor (bold number) with stilbene as the donor in butyronitrile solvent, except where noted. See Experimental Section for estimates of errors. [b] Value used in the determination of k_{fr} and k_{-et} (see text), obtained from experiments on the corresponding *N*-ethyl compound (Table 3), except where noted. [c] WIth tri-p-anisylamine as the donor in acetonitrile solvent. [d] Too small to be considered, see text. [e] With biphenyl as the donor. [f] With 1,2,4-trimethylbenzene as the donor in acetonitrile solvent. Rate constant obtained by direct observation of the radical, does not rely on other measurements, see text. [g] This value represents the sum ($k_{-et} + k_{sep}$), see text. [h] Assumed to be equal to the rate constant obtained for compound **10E**.

Fragmentation Rate Constants. Fragmentation of the radicals from compounds **2** and **12** was slow enough to be measured using conventional nanosecond laser spectroscopy as

(17) Chandler, D. *Introduction To Modern Statistical Mechanics*; Oxford: New York, 1987.

(18) (a) Gould, I. R.; Farid, S. *Acc. Chem. Res.* ,**1996**, *29*, 522. (b) Gould, I. R.; Young, R. H.; Farid, S. *J. Phys. Chem.* **1991**, *95*, 2068. (c) Arnold, B. R.; Atherton, S. J.; Farid, S.; Goodman, J. L.; Gould, I. R. *Photochem. Photobiol*. **1997**, *65*, 15.

(19) Spiegel, M. R. *Theory and Problems of Statistics*; McGraw-Hill: New York, 1961.

Table 3. Rate Constants for Return Electron Transfer, and Separation, for Geminate Pairs of Reduced *N*-Ethylheterocycles at Room Temperature[a]

Structure	Number	k_{-et}, s^{-1}	k_{sep}, s^{-1}
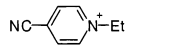	**3E**	1.3×10^{10} [b]	2.9×10^{9} [b]
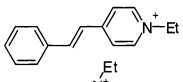	**10E**	1.6×10^{9}	5.7×10^{8}
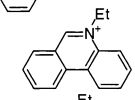	**6E**	2.0×10^{9}	5.6×10^{8}
	**4E**	3.8×10^{9}	9.2×10^{8}
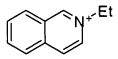	**5E**	1.4×10^{9}	8.2×10^{8}
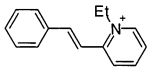	**7E**	1.4×10^{9}	5.2×10^{8}
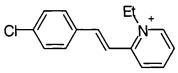	**8E**	1.6×10^{9}	5.5×10^{8}

[a] For charge-transfer complexes of the radical precursor (bold number) with stilbene as the donor in butyronitrile solvent, except where noted. See Experimental Section for estimates of errors. [b] With biphenyl as the donor.

Scheme 8

described above. Measurements as a function of temperature were performed, and the Arrhenius parameters summarized in Table 1 were determined. The rate constant for **2** in 1,2-dichloroethane is reasonably close to the value of 1.4×10^4 s^{-1} reported in the literature in acetonitrile for the corresponding *N*-ethoxy compound.[11a]

The rate constants for fragmentation of the other radicals were determined using the CT excitation methods described above. The elementary rate constants for the CT complexes of the *N*-methoxy compounds and the corresponding *N*-ethyl-derivatives are summarized in Tables 2 and 3. For **1**, the sum of the rate constants for fragmentation and return electron transfer was much larger than that for separation, which was thus ignored. The value obtained for **3** is reasonably similar to that reported previously, 8×10^9 s^{-1}.[11b]

The data exhibit a very wide range of values for k_{fr}, almost 7 orders of magnitude, from 4×10^4 s^{-1} for **2** to 2.7×10^{11} s^{-1} for **1**. Experimental measurements of the temperature dependencies of the reactions for **2** and **12** gave estimates of the barrier heights for these reactions, Table 1. The Arrhenius preexponential factors obtained in these cases (1.75×10^{12} and 1.52×10^{13} s^{-1} for **2** and **12**, respectively) are large. The value for **12** is very close to (kT/h), which is consistent with a unimolecular reaction that occurs efficiently after the energy barrier is surmounted.[20] Assuming that **12** is a reasonable model for the other reactions of Table 2, this would imply that the differences in the rate constants are due mainly to differences in energy barrier heights, the radical from **2** being perhaps an exception. The somewhat smaller preexponential factor here may be a consequence of the fact that the reactive species is a cation, and solvent reorientation effects in the transition state may be important. An additional factor may be the fact that there are degenerate radical states in this case, see further below.

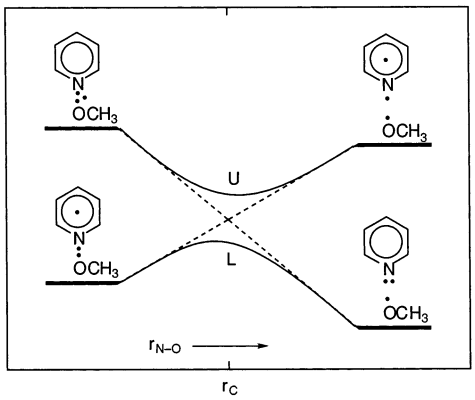

Figure 3. State correlation diagrams for a pure π^* pyridyl radical (bottom left) and a pure σ^* radical (top left) as a function of N−O bond length, r_{N-O}. The dotted lines show the correlations (and lack of avoidance) for the flat geometry. The solid curves show the energies of lower, L, and upper, U, electronic energy states formed by mixing the pure radical states at a geometry in which the N−O bond is bent out of the plane of the aromatic ring. When r_{N-O} is equal to r_C, the curves meet at a conical intersection in the flat conformation.

Qualitatively, the fragmentation rate constants exhibit reasonable trends. The reaction rate constants decrease with increasing strength of the electron-withdrawing group (compare **1** versus **3**, **10** versus **9**, etc.). The reaction rate constants also decrease with increasing delocalization in the aromatic system (compare **1** versus **4**−**6** and **10**). A combination of delocalization and withdrawing groups decreases the rate constant further (compare **3** versus **11**, **1** versus **11**, and **12**, etc.). The extreme case is **2**, which exhibits by far the slowest rate constant for fragmentation. The *p*-(*N*-methoxypyridyl)) is the strongest withdrawing group, but perhaps more importantly, delocalization of this radical is most extensive due to degenerate resonance structures with the radical alternately on each of the two rings, Scheme 8. This is presumably a major reason for relatively slow fragmentation (relatively high radical stability) in this case.

Assuming the thermodynamics and kinetics of the radical fragmentation reactions are related, the thermodynamic cycle of Scheme 2 provides a qualitative explanation for the electron-withdrawing effects, if not the delocalization effects. However, we sought a molecular explanation for the observed rate trends, which requires an examination of the important orbital and state correlations.

Conical Intersection Model for Fragmentation. A useful starting point is the simple-state correlation diagram shown in Figure 3. For simplicity, the simple *N*-methoxypyridinium parent compound (not studied experimentally) is chosen as an illustrative example. For most nitrogen heterocycles, the lowest-energy unoccupied orbital is clearly π^*.[21] The pyridyl radical formed upon reduction of *N*-methoxypyridinium (lower left in Figure 3) is thus shown in the geometry of the cation, with the extra electron associated with the π system (the π^* radical). Increasing

(20) Moore, J. W.; Pearson, R. G. *Kinetics and Mechanism*, 3rd ed.; John Wiley: New York, 1981.

(21) Turner, D. W. *Molecular Photoelectron Spectroscopy: A Handbook of He 584 Å Spectra*; Wiley-Interscience: New York, 1970.

the N−O bond length, r_{N-O}, produces the methoxy radical and pyridine with uncoupled electrons, one localized on an atomic orbital on nitrogen and one in the π system. Thus, bond stretching in the π^* radical leads to an excited state of pyridine and does not correlate with the ground-state reaction products, which are shown on the lower right of Figure 3. *Decreasing* the nitrogen−oxygen bond distance in the ground-state products, that is, *reversing* the fragmentation reaction, leads to a higher-energy pyridyl radical in which the extra electron is in a N−O σ^* orbital (the σ^* radical, top left in Figure 3). The state correlations, indicated by the dashed lines in Figure 3, cross at an N−O bond distance, r_C. Bond fragmentation thus requires a transition from the π^* radical state to the σ^* radical state. This is not possible at the crossing point since the required mixing of the π^* and σ^* orbitals is symmetry-forbidden in the flat configuration of the radical.[22]

Mixing of these orbitals is allowed upon bending of the N−O bond out of the plane of the aromatic ring.[22] In the absence of orbital mixing (pure π^* and pure σ^* radicals), this bending would result in an increase in energy. This is due to increases in the energy of some of the occupied orbitals, described in detail below, and at very large bending angles to electron repulsion effects. For the π^* radical, these energy increases are offset somewhat by a decrease in energy of the singly occupied orbital, see further below. The increases in energy with increasing bending angle, α (defined in Figure 4), for the pure π^* and σ^* radicals are illustrated qualitatively as the dotted curves in Figure 4, for two different values of r_{N-O}. The upper panel of Figure 4 represents the situation at the energy crossing point, r_C. Here, the energies of the pure π^* and σ^* radicals are identical in the flat geometry ($\alpha = 180°$), and the two dotted curves touch. The lower panel in Figure 4 illustrates the situation at a smaller value of r_{N-O}, that is, where the energy of the pure π^* radical is lower than that of the pure σ^* radical.

The important consequence of bending, however, is the π^*/σ^* orbital mixing that produces two new radical states from the π^* and σ^* states. The new states are designated as L for the lower-energy radical state that actually undergoes the fragmentation reaction, and U for the corresponding higher-energy (excited) state, respectively. These are indicated in Figures 3 and 4 by the solid curves. The L state is lower in energy than either of the π^* or σ^* states, and at lower bending angles, an overall stabilization results. Orbital mixing thus decreases the energy of the radical, and opposes the energy-increasing effects of bending described above. The amount of bending in a particular radical will be determined by the extents to which these energy increasing and -decreasing contributions vary with bending angle. The point at which the radical states cross at r_C in Figure 3, and touch in the bending coordinate in Figure 4, defines a conical intersection that the reaction must avoid.[12,23]

The reaction thus proceeds along the lower-energy surface, L, by a combination of N−O stretching and bending motions. The reaction rate will presumably increase with increasing bending angle (up to a point) for one of two possible reasons. When the bending angles are small, the π^*/σ^* mixing is minimal. Under these conditions, the energy splitting between the L and U surfaces around r_C is small, and an unproductive jump from the L to the U surface is possible as r_{N-O} approaches r_C.[24] The reaction rate constant increases with increasing bending since this increases the splitting between the U and L surfaces, and decreases the probability of unproductive jumps from the L to the U surface.[24]

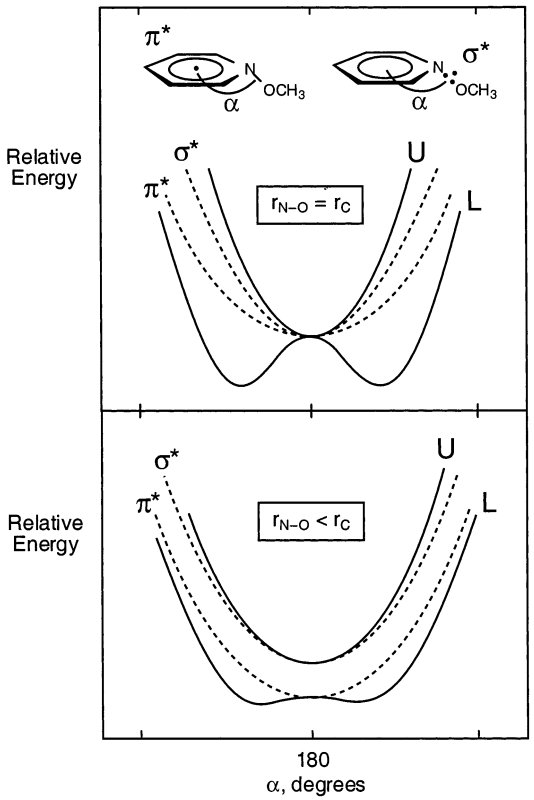

Figure 4. (Dashed lines) Qualitative representation of the energies of pure π^* and σ^* pyridyl radicals as a function of the N−O out-of-plane bending angle α. (Solid lines) Energies of the two radical states, L = lower and U = upper, formed by mixing the pure π^* and σ^* radicals. When the N−O bond length is equal to r_C (top panel), the energies of the two radical configurations are equal in the flat geometry. At smaller N−O bond lengths (lower panel), the energy of the π^* radical is lower than that of the σ^* radical. When r_{N-O} is equal to r_C, the curves meet at a conical intersection.

At larger bending angles the π^*/σ^* mixing is extensive. Under these conditions, the splitting between the L and U surfaces is large and jumps between the surfaces have negligible probability, that is, the reaction becomes adiabatic.[24] Increasing the out-of-plane bending further increases the energy splitting between the U and L states, thus lowering the barrier to reaction and increasing the reaction rate. The large values for the preexponential factors obtained in the temperature dependence studies (Table 1), suggest that the reactions are indeed adiabatic and that the reactions become faster with increased bending for this second reason, that is, due to a lowering of the energy barrier.

To provide further evidence for the conical intersection description of the reaction potential energy surface, ab initio electronic structure calculations were performed. The protonated *N*-methoxypyrazinium radical **14R**, eq 13, was chosen as a model radical for the calculations since it contains both the

(22) Michl, J.; Bonacic-Koutecky, V. *Electronic Aspects of Organic Photochemistry*; Wiley-Interscience: New York, 1990.
(23) The touching of the surfaces in the bending coordinate is a Renner−Teller type interaction.[12a]
(24) (a) Butler, L. J. *Annu. Rev. Phys. Chem.* **1998**, *49*, 125. (b) Salem, L. *Electrons in Chemical Reactions*; Wiley-Interscience: New York, 1982.

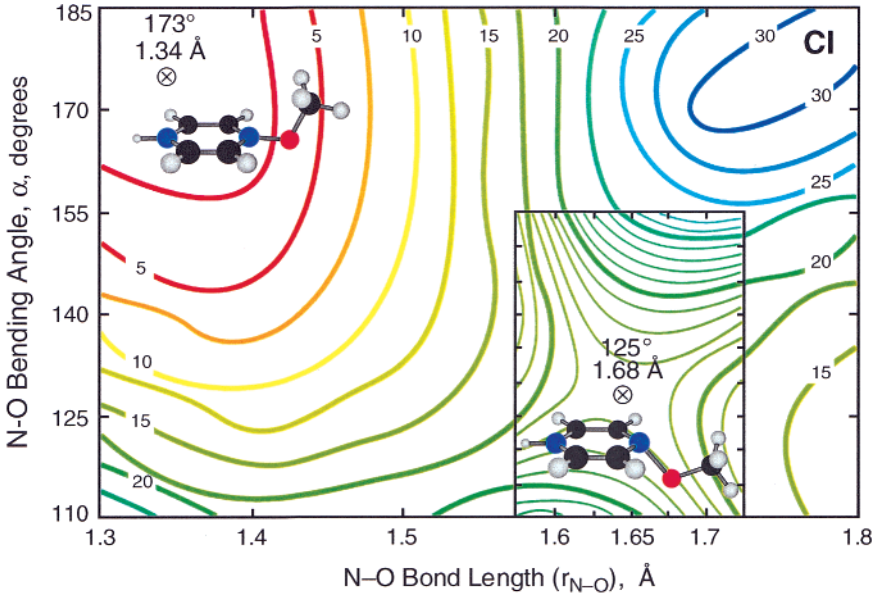

Figure 5. Electronic energy surface for reaction of 4-H^+-1-methoxypyrazinium cation, **14R**, calculated using the UHF/6-31+G* method. The energies, kcal mol^{-1}, are normalized to the energy of the minimized radical structure. The locations, structures, and values for r_{N-O} and α of the radical minimum and the transition state are indicated. The conical intersection (CI) is located at the top right corner.

N-methoxypyridyl structure and a simple and strong withdrawing group.

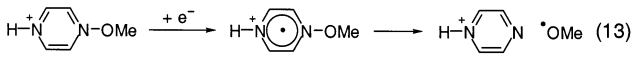

14R

The electronic energy of the radical was computed using the spin-unrestricted Hartree−Fock method (UHF/6-31+G*). Thirty six points were geometry-optimized at different values of the N−O bond length r_{N-O} (from 1.3 to 1.8 Å at 0.1 Å intervals) and the N−O bending angle α (from 110° to 185° at 15° intervals) as indicated by the large, coarse grid of Figure 5. Seventy further points were optimized for r_{N-O} from 1.575 to 1.725 Å at 0.025 Å intervals, and for α from 110° to 155° at 5° intervals in the same way for the fine grid covering the area near the transition state. The points at the different values of r_{N-O} and α were used to construct the potential energy surface indicated by the contour lines in Figure 5. In addition, the minimum and transition state were calculated separately and without constraints, as indicated in the Figure. The Figure very clearly indicates that the reaction path from the minimum to the transition state involves simultaneous N−O bond stretching and bending. The conical interaction was not specifically located, but is clearly at α = 180° and between 1.75 and 1.8 Å, Figure 5.

The data also clearly indicate highly bent transition states for the fragmentation reaction. Thus, the important factors that control the reaction rate should be those that determine the extent of out-of-plane bending and orbital mixing in the bent conformation. The faster reactions will require less energy to reach the bent transition state, and slower reactions will require more energy.

To investigate the role of N−O out-of-plane bending in the reactions, more accurate UB3PW91/6-31+G* density functional electronic structure calculations were performed on several of the fragmenting radicals that were studied experimentally.[25] Minimum-energy configurations for the radicals were obtained in each case. The calculated N−O bond lengths, r_{N-O}, and out-of-plane bending angles, α, are summarized in Figure 6, together with the corresponding rate constants for fragmentation. The results reveal some interesting trends. In general, the N−O bond length in the radical increases with increasing reaction rate, from 1.37 Å for **2** (the slowest fragmenting radical) to 1.43 Å for **1** (the fastest fragmenting radical). Larger effects are seen in the out-of-plane bending angles, which increases significantly with increasing reaction rate. Radical **2** is close to flat (α = 175°), whereas **1** is significantly bent (α = 148°). For a completely sp^3-hybridized nitrogen, α would be ca. 135°.

As discussed above, the varying degrees of bending in the radicals can be understood as arising from varying extents of mixing of the π^* and σ^* orbitals. The orbital energy diagram of Figure 7 provides a useful basis for this discussion. Bending transforms the important molecular orbitals from those of a cyclic π-radical system, π^c, into those of a pentadienyl system, π^p, plus a nonbonding orbital on nitrogen, n. As discussed above, in the absence of π^*/σ^* orbital mixing, the overall energy increases with bending since two electrons (in $\pi_3{}^c$) are raised from a bonding to a nonbonding orbital (n) as the orbital system transforms from π^c to π^p. In the pure π^* radical shown in Figure 7, this is partially offset by the fact that the unpaired electron is lowered from the antibonding $\pi_4{}^c$ to the nonbonding $\pi_3{}^p$ in the pentadienyl system.

These energy-increasing contributions are compensated by the stabilizing effect of orbital mixing. In Figure 7, the most important mixing is illustrated, that is, that between the highest occupied $\pi_3{}^p$ orbital of the pentadienyl system and the relatively low-energy N−O σ^* orbital.[26] The simplest interpretation of the results of the electronic structure calculations is that the extent of this mixing, and thus the energy benefit of out-of-

(25) (a) Becke, A. D. *J. Chem. Phys.* **1993**, *98*, 5648. (b) Hehre, W. J.; Ditchfield, R.; Pople, J. A. *J. Chem. Phys.* **1972**, *56*, 2257. (c) Krishnan, R.; Binkley, J. S.; Seeger, R.; Pople, J. A. *J. Chem. Phys.* **1980**, *72*, 650. (d) McLean, A. D.; Chandler, G. S. *J. Chem. Phys.* **1980**, *72*, 5639.

(26) The $\pi_3{}^p$ orbital is roughly at the nonbonding energy level and thus is not strictly a π^* orbital. To avoid changing notation, however, we will continue to refer to π^*/σ^* mixing.

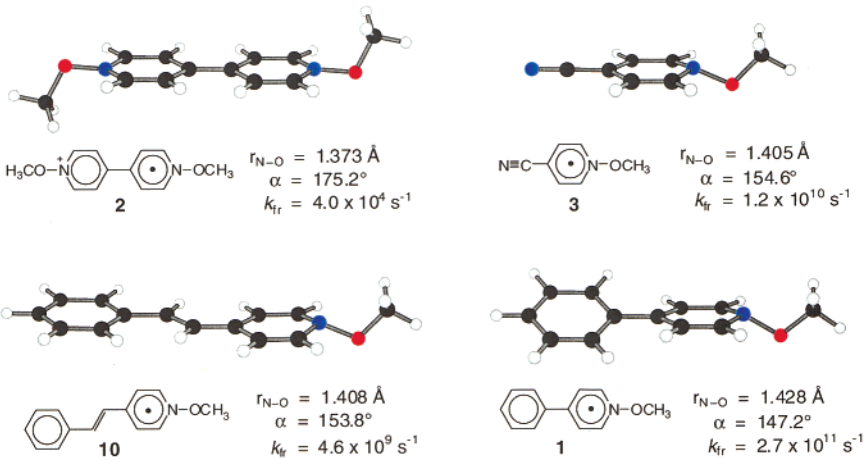

Figure 6. UB3PW91/6-31+G* minimized structures for radicals obtained by one-electron reduction of *N*-methoxyheterocycles (bold numbers), the calculated radical nitrogen−oxygen bond distances, r_{N-O}, the out-of-plane bending angles, α, and the experimental rate constants for N−O bond fragmentation, k_{fr}.

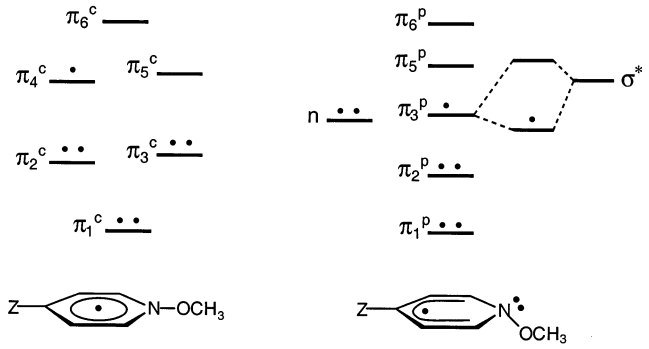

Figure 7. Molecular orbital energy diagram for (left) a flat π^* pyridyl radical and (right) a bent π^* pyridyl radical. The orbitals in the flat conformation are those of a cyclic π system, those in the bent conformation are those of a pentadienyl system plus a nonbonding orbital on nitrogen. Mixing between the π orbitals and the antibonding σ^* orbital of the N−O bond occurs only in the bent conformation.

plane bending, is determined by the effects of the substituents on the important molecular orbitals. The higher the energy of the π_3^p orbital (the closer to that of the σ^* orbital), the greater the mixing.

An electron-withdrawing substituent in the para position of a pyridyl radical, Z in Figure 7, will lower the energies of π_1^c, π_2^c, and π_4^c in the cyclic system but will only lower the energies of π_1^p and π_3^p in the pentadienyl system. Thus, a withdrawing group will stabilize a pure π^* radical more when flat than when bent, since the energies of more electrons are lowered in the flat conformation. Thus, compared to an unsubstituted radical, the energy-increasing contributions to bending are more important with an electron-withdrawing group. Furthermore, by lowering the energy of the π_3^p orbital, mixing with the σ^* orbital is decreased in the bent conformation, and the stabilizing effect of mixing is decreased. Consequently, radicals with electron-withdrawing groups are more planar, more energy is required to reach the bent geometry of the transition state for fragmentation, and their reactions are slower, all as observed.

An electron-donating group will raise the energies of π_1^c, π_2^c, and π_4^c in the cyclic system, and π_1^p and π_3^p in the pentadienyl system. Thus, a donating group will destabilize a pure π^* radical more when flat than when bent (since the energies of more electrons are raised in the flat conformation), and the energy-increasing contributions to bending are less important in this case. Furthermore, because the energy of the π_3^p orbital is raised, mixing with the σ^* orbital is increased. Thus, radicals with electron-donating groups should have a more bent geometry, and thus be closer to the geometry of the transition state for fragmentation, and should react faster.

The effect of delocalizing groups is more subtle. Delocalizing groups reduce the energy gap between the bonding and antibonding orbitals in both the cyclic and the pentadienyl systems. However, in the pentadienyl radical, the unpaired electron is close to the nonbonding energy level (π_3^p in Figure 7), and there is no significant change in the energy of this orbital upon delocalization. Thus, delocalization lowers the energy of the unpaired electron in the flat cyclic radical system and not in the bent pentadienyl radical. Bending in the delocalized radicals is thus associated with a higher energy cost, and consequently the radicals are flatter. The flatter delocalized radicals require more energy to reach the bent geometry of the transition state and fragment more slowly; again, all as observed.

Return Electron Transfer and Separation. In general, the return electron transfer rate constants appear to follow expected trends for electron-transfer reactions in the inverted region.[18a] The main factors that control the rate constant for return electron transfer is the exothermicity of the reaction and, to a lesser extent, the molecular size.[18a] The reaction exothermicity is given by the oxidation potential of the donor and the reduction potential of the acceptor.[18a] Thus, only reactions with the same donor can usefully be compared. In the inverted region, the less negative the reduction potential, the less exothermic the return electron transfer reaction and the larger the rate constant. Although reduction potentials for the various *N*-methoxy and *N*-ethyl-heterocycles are not generally available, some obvious trends can be observed. For example, return electron transfer is significantly faster for the styrylpyridiniums with strong withdrawing groups, **9** and **11** as compared to **10**, as expected.[27] In the inverted region, smaller compounds tend to have larger rate constants for return electron transfer. Although it is difficult to determine the extent to which differences in the rate constants for **4**, **5**, **6**, and **10** are due to differences in reduction potential,

(27) k_{-et} was not determined for **9** and **11**, only the sum ($k_{-et} + k_{sep}$) (Table 2). However, it is clear from Table 3 that the k_{sep} values for the other compounds vary over a small range and are all much smaller than ($k_{-et} + k_{sep}$) for **9** and **11**. Therefore, k_{-et} for **9** and **11** must be much larger than that for **10**.

it is generally true that the smaller compounds undergo return electron transfer with larger rate constants, as expected. Interestingly, return electron transfer is uniformally slower for the *N*-ethyl (Table 3)- compared to the *N*-methoxy-substituted compounds (Table 2). Presumably, the *N*-methoxy compounds are easier to reduce than the *N*-ethyl compounds. Another interesting possible reason for faster return electron transfer for the *N*-methoxy compared to that for the *N*-ethyl radicals is that the change in the N−O bond length upon reduction of the former is presumably much larger than the corresponding change in the N−C bond length in the latter. Return electron transfer for the *N*-methoxy radicals will thus be characterized by a larger internal reorganization energy, which will also contribute to an increase in the rate constant for return electron transfer in the inverted region.[18a]

The rate constants for separation do not vary over a very wide range, from ca. $6-30 \times 10^8$ s^{-1}, Table 2. In general, the rate constants are larger for the smaller compounds. A full discussion of the factors controlling the rate constants for separation will be published elsewhere.[28]

Conclusions

N−O bond fragmentation of radicals formed by one-electron reduction of *N*-methoxy-substituted aromatic compounds occurs with rate constants that can vary over a very wide range, from 4.0×10^4 to 2.7×10^{11} s^{-1} for those radicals studied here. The reaction requires mixing of π^* and σ^* orbitals,[26] which is achieved by bending the N−O bond out of the plane of the aromatic ring. Substituent and delocalization effects on the reacting radicals can be understood in terms of varying extents of this orbital mixing. Extensive mixing leads to a radical that is close in geometry and energy to the bent transition state for reaction. Strong electron-withdrawing groups or delocalizing structures or both result in decreased π^*/σ^* orbital mixing and slow the reactions. The discussion above suggests that electron-donating groups should increase the extent of π^*/σ^* orbital mixing so that fragmentation may be even faster than the fastest reactions observed here. We are currently exploring structures of this type to confirm this prediction, with the ultimate goal of discovering radical fragmentation reactions that occur with no energy barrier.[29]

The orbital mixing results in a conical intersection that the reaction avoids. Although the important role of conical intersections in photochemical processes is well documented,[30] there have been very few discussions of conical intersections in ground-state thermal reactions of organic species,[31] and to the best of our knowledge, none at all for reactions of neutral organic radicals in solution. We are in the process of further exploring the role of the conical intersection in these reactions using more extensive electronic structure calculations.[29]

Experimental Section

Materials. The solvents were spectrograde from Aldrich and were used as received. 9,10-Dicyanoanthracene and *p*-trianisylamine were gifts from Samir Farid (Eastman Kodak Company) and used as received. Stilbene, biphenyl, 1,2,4-trimethylbenzene, and benzyltrimethylsilane were obtained from Aldrich and were used as received. 9-Thioxanthenone was obtained from Aldrich, and was recrystallized from ethanol.

General Synthetic Procedures. The *N*-ethyl- and *N*-methoxy heterocycles were prepared by alkylation of the corresponding heterocycles and heterocycle *N*-oxides. The compounds were characterized by proton and carbon NMR spectroscopy using the Varian Gemini 300, Varian Inova 400, and Varian Inova 500 spectrometers. The samples were dissolved in $CDCl_3$, DMSO-d_6, CD_3CN, or CD_3OD (Cambridge Isotopes). Mass verification was accomplished using a Vestec MALDI-TOF mass spectrometer with 337-nm excitation; the compounds were sometimes excited without a matrix (LD-TOF). Melting points are uncorrected.

General Procedures for the Heterocycles. Quinoline, isoquinoline, phenanthridine, 4-benzoylpyridine, and 4-cyanopyridine were obtained from Aldrich and used as received. 2-Styrylpyridine and 2-(4-chlorostyryl)pyridine were gifts from Samir Farid (Eastman Kodak Company) and were used as received. The other styrylpyridines were prepared using the condensation procedure of Williams, et al.[32]

General Procedures for the *N*-Oxides. Quinoline *N*-oxide (Aldrich), isoquinoline *N*-oxide (Aldrich), 4,4'-dipyridyl-*N*,*N*'-dioxide (Aldrich), and 4-cyanopyridine *N*-oxide (Lancaster) were obtained commercially and used as received. Phenanthridine *N*-oxide was prepared according to the method of Hayashi and Hotta.[33] The other *N*-oxides were prepared using the following general procedure.[34] The heteroaromatic compound (6 mmol) was dissolved in 35 mL of glacial acetic acid in a 100-mL round-bottom flask. After the addition of 8 mmol H_2O_2 (30% solution) the mixture was held at 80 °C for 12 h. After cooling to room temperature, the mixture was poured into chloroform and extracted successively with an aqueous solution of HCl, an aqueous solution of sodium hydroxide, and then brine. The organic phase was dried over magnesium sulfate, and the solvent was removed. The crude *N*-oxides were alkylated without further purification.

General Procedures for the *N*-Ethyl Heterocycles. The *N*-ethyl heterocycles were prepared according to the following general procedure. A mixture of 1.15 equiv of triethyloxonium hexafluorophosphate (Aldrich) and 1 equiv of the *N*-heterocycle was stirred in dichloromethane under argon for 4 h. After the addition of 15 mL of methanol the solvent was removed, and the crude product was recrystallized.

General Procedures for the *N*-Methoxy Heterocycles. *N*-Methoxy-4-(4-cyanostyryl)pyridinium tetrafluoroborate and *N*-methoxy-4-phenylpyridinium tetrafluoroborate were gifts from Samir Farid (Eastman Kodak Company) and were used as received. The others were prepared according to the following general procedure. A mixture of 1.15 equiv of trimethyloxonium tetrafluoroborate (Aldrich) and 1 equiv of the heterocycle *N*-oxide was stirred in dichloromethane under argon for 4 h. After the addition of 15 mL of methanol the solvent was removed, and the crude product was recrystallized.

4-Styrylpyridine. Following the literature procedure,[32] 4-picoline (6.0 g, 64.4 mmol) and benzaldehyde (6.84 g, 64.4 mmol) were refluxed 12 h in 35 mL of acetic anhydride to give 5.50 g (30.3 mmol, 47%) of 4-styrylpyridine. Mp 121−123 °C. ^{1}H NMR (300 MHz, $CDCl_3$) δ

(28) Lorance, E. D.; Gould, I. R. Manuscript in preparation.
(29) Lorance, E. D.; Kramer, W. H.; Hendrickson, K. A.; Gould, I. R. Manuscript in preparation.
(30) See, for example: (a) Klessinger, M. *J. Photochem. Photobiol. A* **2001**, *144*, 217. (b) De Vico, L.; Page, C. S.; Garavelli, M.; Bernardi, F.; Basosi, R.; Olivucci, M. *J. Am. Chem. Soc.* **2002**, *124*, 4124. (c) Ben-Nun, M.; Molnar, F.; Schulten, K.; Martinez, T. J. *Proc. Natl. Acad. Sci. U.S.A.* **2002**, *99*, 1769. (d) Clifford, S.; Bearpark, M. J.; Bernardi, F.; Olivucci, M.; Robb, M. A.; Smith, B. R. *J. Am. Chem. Soc.* **1996**, *118*, 7353. (e) Wilsey, S.; Houk, K. N. *J. Am. Chem. Soc.* **2000**, *122*, 2651. (f) Yamamoto, N.; Olivucci, M.; Celani, P.; Bernardi, F.; Robb, M. A. *J. Am. Chem. Soc.* **1998**, *120*, 2407. (g) Wilsey, S.; Houk, K. N.; Zewail, A. H. *J. Am. Chem. Soc.* **1999**, *121*, 5772. (h) Zhong, D.; Diau, E. W.-G.; Bernhardt, T.; De Feyter, S.; Roberts, J. D.; Zewail, A. H. *Chem. Phys. Lett.* **1998**, *298*, 129.
(31) (a) Blancafort, L.; Jolibois, F.; Olivucci, M.; Robb, M. A. *J. Am. Chem. Soc.* **2001**, *123*, 722. (b) Bearpark, M. J.; Robb, M. A.; Yamamoto, N. *Spectrochim. Acta, Part A* **1999**, *55*, 639. (c) Blancafort, L.; Adam, W.; Gonzalez, D.; Olivucci, M.; Vreven, T.; Robb, M. A. *J. Am. Chem. Soc.* **1999**, *121*, 10583. (d) Diau, E. W.-G.; De Feyter, S.; Zewail, A. H. *Chem. Phys. Lett.* **1999**, *304*, 134.
(32) Williams, J. L. R.; Adel, R. E.; Carlson, J. M.; Reynolds, G. A.; Borden, D. G.; Ford, J. A. *J. Org. Chem.* **1963**, *28*, 387.
(33) E. Hayashi, Y. Hotta, *J. Pharm. Soc. Jpn.* **1960**, *80*, 834.
(34) Katritzky, A. R.; Lagowski, J. M. *Chemistry of the Heterocyclic N-Oxides*; Academic: New York, 1971.

(ppm) = 6.98 (d, 1 H, J = 16.5 Hz), 7.25 (d, 1 H, J = 16.5 Hz), 7.31−7.40 (m, 5 H), 7.51 (dd, 2 H, J = 1.2, 8.1 Hz), 8.55 (d, 2 H, J = 6.3 Hz). ^{13}C NMR (75 MHz, $CDCl_3$) δ (ppm) = 120.8, 125.9, 126.9, 128.7, 128.8, 133.2, 136.1, 144.6, 150.0.

4-(4-Nitrostyryl)pyridine. Following the literature procedure,[32] 4-picoline (3.08 g, 33.1 mmol) and 4-nitrobenzaldehyde (5.00 g, 33.1 mmol) were refluxed 12 h in 17 mL of acetic anhydride to give 4.32 g (19.1 mmol, 58%) of 4-(4-nitrostyryl)pyridine. Mp 166−168 °C. ^{1}H NMR (300 MHz, $CDCl_3$) δ (ppm) = 7.14 (d, 1 H, J = 16.5 Hz), 7.31 (d, 1 H, J = 16.5 Hz), 7.36−7.39 (m, 2 H), 7.63−7.66 (m, 2 H), 8.17−8.21 (m, 2 H), 8.59 (br d, 2 H). ^{13}C NMR (75 MHz, $CDCl_3$) δ (ppm) = 121.0, 124.1, 127.4, 130.3, 130.6, 142.4, 143.4, 147.4, 150.2.

4-(2,3,4,5,6-Pentafluorostyryl)pyridine. Following the literature procedure,[32] 4-picoline (0.70 g, 7.65 mmol) and pentafluorobenzaldehyde (1.5 g, 7.65 mmol) were stirred 4 d in 15 mL of acetic anhydride. The resulting solid was purified by column chromatography (silica gel, methanol/dichloromethane 1:30, R_f = 0.4) to give 0.5 g (1.84 mmol, 24%) of 4-(2,3,4,5,6-pentafluorostyryl)pyridine. Mp 113−115 °C. ^{1}H NMR (300 MHz, $CDCl_3$) δ (ppm) = 7.15 (d, 1 H, J = 13.6 Hz), 7.33 (d, 1 H, J = 13.6 Hz), 7.36 (d, 2 H, J = 4.8 Hz), 8.61 (d, 2 H, J = 4.0 Hz). ^{13}C NMR (75 MHz, $CDCl_3$) δ (ppm) = 111.3, 117.2, 121.0, 134.4, 137.8, 140.5, 143.7, 145.0, 150.3. ^{19}F NMR (470.9 MHz, $CDCl_3$ (versus NaF in D_2O)) δ (ppm) = −42.01 (dt, 2 F), −33.92 (t, 1 F), −21.59 (dd, 2 F). MS m/z 272.4 ($(M + H)^+$).

***N,N'*-Dimethoxy-4,4'-dipyridylium Bis-tetrafluoroborate (2).** Following the general procedure, trimethyloxonium tetrafluoroborate (847 mg, 5.70 mmol) and 4,4'-dipyridyl *N*,*N*'-dioxide (511 mg, 2.49 mmol) were stirred in 10 mL of acetonitrile for 4 h. Recrystallization from acetonitrile afforded 746 mg (1.90 mmol, 76%) of **2**. ^{1}H NMR (300 MHz, CD_3OD(+CD_3CN)) δ (ppm) = 4.55 (s, 6 H), 8.60−8.64 (m, 4 H), 9.43−9.45 (m, 4 H). ^{13}C NMR (75 MHz, CD_3OD(+CD_3CN)) δ (ppm) = 69.0, 116.6, 127.8, 141.0. MS m/z 187.2 ($(M - OCH_3)^+$).

***N*-Methoxy-4-cyanopyridinium Tetrafluoroborate (3).** Following the general procedure, trimethyloxonium tetrafluoroborate (0.72 g, 4.87 mmol) and 4-cyanopyridine *N*-oxide (0.56 g, 4.63 mmol) were stirred in 30 mL of dichloromethane for 4 h. Recrystallization from methanol afforded 0.81 g (3.65 mmol, 79%) of **3**. ^{1}H NMR (300 MHz, DMSO-d_6) δ (ppm) = 4.48 (s, 3 H), 8.83 (d, 2 H, J = 6.6 Hz), 9.75 (d, 2 H, J = 6.6 Hz). ^{13}C NMR (75 MHz, DMSO-d_6) δ (ppm) = 69.7, 114.6, 126.1, 132.6, 142.2. MS m/z 135.3 (M^+).

***N*-Ethyl-4-cyanopyridinium Hexafluorophosphate (3E).** Following the general procedure, triethyloxonium hexafluorophosphate (0.65 g, 2.62 mmol) and 4-cyanopyridine (0.24 g, 2.27 mmol) were stirred in 30 mL of dichloromethane for 4 h. Recrystallization from methanol/dichloromethane afforded 0.36 g (1.29 mmol, 57%) of **3E**. ^{1}H NMR (300 MHz, DMSO-d_6) δ (ppm) = 1.55 (t, 3 H, J = 7.2 Hz), 4.68 (q, 2 H, J = 7.2 Hz), 8.69 (d, 2 H, J = 6.6 Hz), 9.35 (d, 2 H, J = 6.6 Hz). ^{13}C NMR (75 MHz, DMSO-d_6) δ (ppm) = 16.0, 57.5, 114.8, 126.9, 130.9, 146.0. MS m/z 133.2 (M^+).

***N*-Methoxyquinolinium Tetrafluoroborate (4)**. Following the general procedure, trimethyloxonium tetrafluoroborate (4.09 g, 27.7 mmol) and quinoline *N*-oxide (3.65 g, 25.1 mmol) were stirred in 110 mL of dichloromethane for 4 h. Recrystallization from methanol/dichloromethane afforded 3.80 g (15.4 mmol, 61%) of **4**. ^{1}H NMR (300 MHz, CD_3OD) δ (ppm) = 4.60 (s, 3 H), 8.07−8.18 (m, 2 H), 8.34 (t, 1 H, J = 7.8 Hz), 8.48 (d, 1 H, J = 8.1 Hz), 8.59 (d, 1 H, J = 8.7 Hz), 9.23 (d, 1 H, J = 8.1 Hz), 9.76 (d, 1 H, J = 6.6 Hz). ^{13}C NMR (75 MHz, CD_3OD) δ (ppm) = 70.5, 117.3, 123.3, 131.5, 132.3, 132.7, 137.7, 138.2, 145.1, 148.0. MS m/z 160.3 (M^+).

***N*-Ethylquinolinium Hexafluorophosphate (4E).** Following the general procedure, triethyloxonium hexafluorophosphate (9.30 g, 37.0 mmol) and quinoline (4.00 g, 31.0 mmol) were stirred in 60 mL of dichloromethane for 4 h. Recrystallization from methanol/dichloromethane afforded 6.62 g (21.8 mmol, 70%) of **4E**. ^{1}H NMR (300 MHz, $CDCl_3$) δ (ppm) = 1.73 (t, 3 H, J = 7.2 Hz), 5.15 (q, 2 H, J = 7.2 Hz), 7.99 (dd, 1 H), 8.10 (dd, 1 H), 8.26 (dt, 1 H), 8.40 (d, 1 H), 8.56 (d, 1 H), 9.19 (d, 1 H), 9.49 (d, 1 H). ^{13}C NMR (75 MHz, $CDCl_3$) δ (ppm) = 13.7, 52.8, 117.7, 121.5, 129.2, 129.6, 130.2, 135.2, 137.1, 146.4, 148.6. MS m/z 158.3 (M^+).

***N*-Methoxyisoquinolinium Tetrafluoroborate (5).** Following the general procedure, trimethyloxonium tetrafluoroborate (4.48 g, 30.3 mmol) and isoquinoline *N*-oxide (4.00 g, 27.6 mmol) were stirred in 120 mL of dichloromethane for 4 h. Recrystallization from ethyl acetate afforded 6.40 g (25.9 mmol, 94%) of **5**. ^{1}H NMR (300 MHz, CD_3OD) δ (ppm) = 4.56 (s, 3 H), 8.06−8.11 (m, 1 H), 8.21−8.27 (m, 1 H), 8.34 (dd, 1 H, J = 1.2, 8.1 Hz), 8.49 (dd, 1 H, J = 1.2, 8.1 Hz), 8.57 (d, 1 H, J = 7.2 Hz), 8.89−8.93 (m, 1 H), 10.20 (d, 1 H, J = 1.8 Hz). ^{13}C NMR (75 MHz, CD_3OD) δ (ppm) = 70.3, 118.5, 128.7, 129.0, 131.2, 132.3, 133.0, 138.1, 138.3, 145.5. MS m/z 160.6 (M^+).

***N*-Ethylisoquinolinium Hexafluorophosphate (5E).** Following the general procedure, triethyloxonium hexafluorophosphate (5.81 g, 23.4 mmol) and isoquinoline (2.50 g, 19.4 mmol) were stirred in 60 mL of dichloromethane for 4 h. Recrystallization from methanol/dichloromethane afforded 4.10 g (13.5 mmol, 70%) of **5E**. ^{1}H NMR (300 MHz, CD_3OD) δ (ppm) = 1.71 (t, 3 H, J = 7.2 Hz), 4.77 (q, 2 H, J = 7.2 Hz), 8.00 (dt, 1 H, J = 0.9, 8.1 Hz), 8.14−8.26 (m, 2 H), 8.39−8.46 (m, 2 H), 8.59 (dd, 1 H, J = 0.9, 6.6 Hz), 9.78 (s, 1 H). ^{13}C NMR (75 MHz, CD_3OD) δ (ppm) = 16.5, 58.3, 127.6, 128.4, 129.3, 131.5, 132.5, 135.3, 138.2, 138.9, 150.6. MS m/z 158.3 (M^+).

***N*-Methoxyphenanthridinium Tetrafluoroborate (6).** Following the general procedure, trimethyloxonium tetrafluoroborate (1.42 g, 9.6 mmol) and phenanthridine *N*-oxide (1.7 g, 8.7 mmol) were stirred in 40 mL of dichloromethane for 4 h. Recrystallization from methanol afforded 2.1 g (7.1 mmol, 81%) of **6**. ^{1}H NMR (500 MHz, CD_3OD at 55 °C) δ (ppm) = 4.67 (s, 3 H), 8.08−8.20 (m, 3 H), 8.38 (dt, 1 H, J = 1.5, 7.8 Hz), 8.58 (dt, 2 H, J = 1.0, 8.0 Hz), 9.02 (d, 1 H, J = 8.5 Hz), 9.07 (d, 1 H, J = 8.0 Hz), 10.46 (s, 1 H). ^{13}C NMR (125 MHz, CD_3OD at 55 °C) δ (ppm) = 70.3, 118.4, 124.5, 125.1, 125.9, 128.7, 131.9, 132.7, 133.2, 133.8, 133.9, 135.8, 139.6, 149.7. MS m/z 210.5 (M^+).

***N*-Ethylphenanthridinium Hexafluorophosphate (6E).** Following the general procedure, triethyloxonium hexafluorophosphate (3.10 g, 11.3 mmol) and phenanthridine (1.98 g, 11.0 mmol) were stirred in 25 mL of dichloromethane for 4 h. Recrystallization from chloroform/acetonitrile afforded 4.10 g (13.5 mmol, 76%) of **6E**. ^{1}H NMR (500 MHz, DMSO-d_6) δ (ppm) = 1.71 (t, 3 H, J = 7.2 Hz), 5.13 (q, 2 H, J = 7.2 Hz), 8.07−8.16 (m, 3 H), 8.38 (t, 1 H, J = 7.2 Hz), 8.56 (d, 1 H, J = 8.7 Hz), 8.62 (d, 1 H, J = 8.1 Hz), 9.10 (d, 1 H, J = 8.7 Hz), 9.13−9.17 (m, 1 H), 10.29 (s, 1 H). ^{13}C NMR (125 MHz, DMSO-d_6) δ (ppm) = 14.7, 53.3, 119.8, 123.0, 123.7, 124.9, 125.8, 130.2, 132.0, 132.7, 132.9, 134.2, 137.8, 155.1. MS m/z 208.3 (M^+).

***N*-Methoxy-2-styrylpyridinium Tetrafluoroborate (7).** Following the general procedure, trimethyloxonium tetrafluoroborate (1.07 g, 7.30 mmol) and 2-styrylpyridine *N*-oxide (1.20 g, 6.08 mmol) were stirred in 30 mL of dichloromethane for 4 h. Recrystallization from methanol afforded 1.35 g (4.51 mmol, 74%) of **7**. ^{1}H NMR (300 MHz, CD_3OD (+CD_3CN)) δ (ppm) = 4.40 (s, 3 H), 7.49−7.52 (m, 3 H), 7.59 (d, 1 H, J = 14.4 Hz), 7.81−7.85 (m, 2 H), 7.91 (dt, 1 H, J = 1.5, 7.2 Hz), 8.06 (d, 1 H, J = 14.4 Hz), 8.44 (dt, 1 H, J = 1.8, 7.2 Hz,), 8.53 (dd, 1 H, J = 1.8, 8.4 Hz), 9.03 (dd, 1 H, J = 1.5, 6.6 Hz). ^{13}C NMR (75 MHz, CD_3OD (+CD_3CN)) δ (ppm) = 70.1, 113.9, 126.9, 127.6, 129.8, 130.3, 132.5, 135.8, 141.7, 145.0, 146.7, 151.6. MS m/z 212.6 (M^+).

***N*-Ethyl-2-styrylpyridinium Hexafluorophosphate (7E).** Following the general procedure, triethyloxonium hexafluorophosphate (2.46 g, 9.93 mmol) and 2-styrylpyridine (1.50 g, 8.28 mmol) were stirred in 40 mL of dichloromethane for 4 h. Recrystallization from methanol/dichloromethane afforded 1.90 g (12.4 mmol, 65%) of **7E**. ^{1}H NMR (300 MHz, CD_3CN) δ (ppm) = 1.59 (t, 3 H, J = 7.8 Hz), 4.75 (q, 2 H, J = 7.8 Hz), 7.45−7.52 (m, 4 H), 7.78−7.88 (m, 4 H), 8.35−8.46 (m, 2 H), 8.73 (d, 1 H, J = 6 Hz). ^{13}C NMR (75 MHz, CD_3CN) δ (ppm) = 15.8, 55.1, 117.7, 126.9, 127.4, 129.6, 130.2, 132.0, 136.0, 145.5, 145.8, 145.9, 153.9. MS m/z 210.3 (M^+).

***N*-Methoxy-2-(4-chlorostyryl)pyridinium Tetrafluoroborate (8).** Following the general procedure, trimethyloxonium tetrafluoroborate (0.95 g, 6.45 mmol) and 2-(4-chlorostyryl)pyridine *N*-oxide (1.30 g, 5.61 mmol) were stirred in 30 mL of dichloromethane for 4 h. Recrystallization from methanol afforded 1.23 g (3.69 mmol, 66%) of **8**. ^{1}H NMR (300 MHz, CD_3OD) δ (ppm) = 4.39 (s, 3 H), 7.45−7.50 (m, 2 H), 7.56 (d, 1 H, J = 15.9 Hz), 7.75−7.82 (m, 2 H), 8.00 (d, 1 H, J = 15.9 Hz), 8.30−8.52 (m, 2 H), 8.68 (d, 1 H, J = 6 Hz), 9.03 (d, 1 H, J = 6.9 Hz). ^{13}C NMR (75 MHz, CD_3OD) δ (ppm) = 68.3, 112.8, 116.6, 125.2, 126.0, 128.5, 129.4, 132.7, 139.9, 143.3, 144.0, 149.5. MS *m*/*z*, 246.4, 248.4 (M^+).

***N*-Ethyl-2-(4-chlorostyryl)pyridinium Hexafluorophosphate (8E).** Following the general procedure, triethyloxonium hexafluorophosphate (217 mg, 0.88 mmol) and 2-(4-chlorostyryl)pyridine (156 mg, 0.72 mmol) were stirred in 5 mL of dichloromethane for 4 h. Recrystallization from methanol/dichloromethane afforded 215 mg (0.55 mmol, 76%) of **8E**. ^{1}H NMR (300 MHz, DMSO-d_6) δ (ppm) = 1.60 (t, 3 H, J = 7.8 Hz), 4.76 (q, 2 H, J = 7.8 Hz), 7.51 (d, 1 H, J = 15.9 Hz), 7.50−7.52 (m, 2 H), 7.78 (d, 1 H, J = 15.9 Hz), (d, 1 H, J = 15.9 Hz), (d, 1 H, J = 15.9 Hz), 7.78−7.81 (m, 2 H), 7.89 (dt, 1 H, J = 1.2, 6.9 Hz), 8.38 (d, 1 H, J = 7.2 Hz), 8.43−8.49 (m, 1 H), 9.35 (d, 1 H, J = 6.3 Hz). ^{13}C NMR (75 MHz, DMSO-d_6) δ (ppm) = 15.5, 53.3, 117.8, 125.8, 129.0, 130.2, 133.7, 135.2, 141.9, 144.5, 145.2, 151.4, 152.6. MS *m*/*z* 244.8, 246.8 (M^+).

***N*-Methoxy-4-(2,3,4,5,6-pentafluorostyryl)pyridinium Tetrafluoroborate (9).** Following the general procedure, trimethyloxonium tetrafluoroborate (199 mg, 1.35 mmol) and 4-(2,3,4,5,6-pentafluorostyryl)pyridine *N*-oxide (322 mg, 1.12 mmol) were stirred in 40 mL of dichloromethane for 4 h. 310 mg (0.80 mmol, 71%) of **9** was obtained as a colorless oil. ^{1}H NMR (400 MHz, CD_3CN) δ (ppm) = 4.39 (s, 3 H), 7.62 (s, 2 H), 8.22 (d, 2 H), 8.88 (dd, 2 H). ^{13}C NMR (75 MHz, CD_3CN) δ (ppm) = 70.8, 126.5, 127.2, 128.6, 131.2, 139.1, 141.6, 142.9, 146.7, 153.4. ^{19}F NMR (470.9 MHz, $CDCl_3$ (versus NaF in D_2O)) δ (ppm) = −38.5 (dt, 2 F), −28.1 (t, 1 F), −25.9 (s, 3 F), −25.2 (s, 1 F), −15.9 (dd, 2 F).

***N*-Methoxy-4-styrylpyridinium Tetrafluoroborate (10).** Following the general procedure, trimethyloxonium tetrafluoroborate (1.25 g, 8.52 mmol) and 4-styrylpyridine *N*-oxide (1.40 g, 7.10 mmol) were stirred in 30 mL of dichloromethane for 4 h. Recrystallization from methanol afforded 1.26 g (4.21 mmol, 59%) of **10**. ^{1}H NMR (300 MHz, CD_3CN) δ (ppm) = 4.35 (s, 3 H), 7.36 (d, 1 H, J = 16.5 Hz), 7.45−7.47 (m, 3 H), 7.69−7.72 (m, 2 H), 7.81 (d, 1 H, J = 16.5 Hz), 8.08 (d, 2 H, J = 7.2 Hz), 8.76 (d, 2 H, J = 7.2 Hz). ^{13}C NMR (75 MHz, CD_3CN) δ (ppm) = 70.7, 123.5, 126.0, 129.3, 130.2, 131.9, 136.0, 141.1, 143.2, 154.8. MS *m*/*z* 212.4 (M^+).

***N*-Ethyl-4-styrylpyridinium Hexafluorophosphate (10E).** Following the general procedure, triethyloxonium hexafluorophosphate (6.70 g, 26.7 mmol) and 4-styrylpyridine (4.00 g, 22.1 mmol) were stirred in 100 mL of dichloromethane for 4 h. Recrystallization from methanol afforded 5.10 g (14.3 mmol, 65%) of **10E**. ^{1}H NMR (300 MHz, CD_3OD) δ (ppm) = 1.62 (t, 3 H, J = 7.2 Hz), 4.55 (q, 2 H, J = 7.2 Hz), 7.39 (d, 1 H, J = 16.5 Hz), 7.42−7.46 (m, 3 H), 7.71−7.74 (m, 2 H), 7.88 (d, 1 H, J = 16.5 Hz), 8.13 (d, 2 H, J = 6.6 Hz), 8.73 (d, 2 H, J = 6.6 Hz). ^{13}C NMR (75 MHz, CD_3OD) δ (ppm) = 14.5, 55.3, 121.8, 123.4, 127.2, 127.4, 128.1, 129.7, 140.8, 142.8, 153.4. MS *m*/*z* 210.3 (M^+).

***N*-Methoxy-4-(4-nitrostyryl)pyridinium Tetrafluoroborate (12).** Following the general procedure, trimethyloxonium tetrafluoroborate (463 mg, 3.13 mmol) and 4-(4-nitrostyryl)pyridine *N*-oxide (690 mg, 2.85 mmol) were stirred in 20 mL of dichloromethane for 4 h. Recrystallization from methanol afforded 610 mg (1.77 mmol, 62%) of **12**. ^{1}H NMR (300 MHz, CD_3CN) δ (ppm) = 4.38 (s, 3 H), 7.52 (d, 1 H, J = 16.5 Hz), 7.84 (d, 1 H, J = 16.5 Hz), 7.88 (d, 2 H, J = 8.7 Hz), 8.16 (d, 2 H, J = 7.2 Hz), 8.26 (d, 2 H, J = 8.7 Hz), 8.84 (d, 2 H, J = 7.2 Hz). ^{13}C NMR (75 MHz, CD_3CN) δ (ppm) = 70.6, 125.1, 126.7, 127.3, 129.9, 139.9, 141.3, 142.0, 149.5, 153.2. MS *m*/*z* 257.1 (M^+).

***N*-Methoxy-4-benzoylpyridinium Tetrafluoroborate (13)** Following the general procedure, trimethyloxonium tetrafluoroborate (2.19 g, 14.8 mmol) and 4-benzoylpyridine *N*-oxide (2.56 g, 12.6 mmol) were stirred in 50 mL of dichloromethane for 4 h. Recrystallization from methanol/dichloromethane afforded 3.41 g (11.3 mmol, 90%) of **13**. ^{1}H NMR (300 MHz, CD_3CN) δ (ppm) = 4.49 (s, 3 H), 7.57−7.62 (m, 2 H), 7.73−7.85 (m, 3 H), 8.26 (dd, 2 H, J = 1.8, 5.1 Hz), 9.14 (dd, 2 H, J = 1.5, 4.8 Hz). ^{13}C NMR (75 MHz, CD_3CN) δ (ppm) = 70.9, 129.6, 129.9, 131.1, 135.0, 135.8, 142.3, 152.6, 192.1. MS *m*/*z* 214.2 (M^+).

Methods. The nanosecond and microsecond time-resolved absorption measurements were performed using a nanosecond transient absorption spectrometer of conventional design.[35] The excitation source was an Opotek Vibrant OPO laser. Typical specifications were pulse width of ca. 4 ns, variable wavelength from 385 to 410 nm and energies in the range 0.5−2 mJ per pulse. The optical densities of the solutions at the excitation wavelengths were adjusted to be ca. 1.0, or as close to 1.0 as possible in a 1-cm path length.

Measurements on the picosecond time scale were also performed using an apparatus of conventional design.[35] The source was a Continuum custom model PY-61C Nd:YAG laser. The specifications at 1064 nm were typically 30 mJ and ca. 6 ps. Frequency tripled 355-nm light was used to excite the sample, either directly or after frequency shifting to 395 or 445 nm using stimulated Raman scattering in cyclohexane. Residual 1064-nm light was used to generate the quasi-continuum white light pulse. The detector was a Princeton Instruments dual diode array detector, controlled by a Princeton Instruments model ST-121S controller. The white light was dispersed using an Acton Research Corp. Spectropro-300i spectrograph. At each setting of an optical delay line, the entire spectrum was recorded from ca. 400 to 800 nm. Integral regions were chosen from these spectra and plotted versus time to give the kinetic data. Experimental details, including excitation and observation wavelengths are provided as Supporting Information.

The measurements of the complex of **1** with *p*-trianisylamine on the subpicosecond time scale were performed using an apparatus that has been previously described.[36] The excitation wavelength used was 420 nm. The kinetics of the geminate pairs were determined by plotting the integrated absorbance of the *p*-trianisylamine band over the range 659−797 nm as a function of time. This integral was used to account for time-dependent spectral shifts in the absorption due to dynamic solvent relaxation.[37]

Errors in the various rate constants were estimated mainly from repeated measurements. On this basis, the errors in the activation parameters for **2** and **12** are estimated to be ca. 15% for the log A values, and ca. 5% for the E_a values. For the radical precursors included in Tables 2 and 3, some experiments were repeated multiple times, and others were repeated with more than one donor and in some cases more than one solvent (detailed data not reported here). Different statistical errors were computed for different radicals where enough repeat experiments were performed. On this basis, an average error of ca. 10% is estimated for all of the rate constants included in the Tables. An exception is the radical from **13**. In this case, the corresponding *N*-ethyl compound was not available, and it was assumed that the value of k_{sep} from compound **10E** was appropriate. On the basis of the variation in the k_{sep} values in Table 3, a maximum error of ca. 25% is estimated for the rate constant in this case.

(35) Herkstroeter, W. G.; Gould, I. R. In *Physical Methods of Chemistry Series*, 2nd ed.; Rossiter, B., Baetzold, R., Eds.; Wiley: New York, 1993; Vol. 8, p 225.
(36) Sakomura, M.; Lin, S.; Moore, T. A.; Moore, A. L.; Gust, D.; Fujihira, M. *J. Phys. Chem. A* **2002**, *106*, 2218.
(37) Barbara, P. F.; Jarzeba, W. *Adv. Photochem.* **1990**, *15*, 1.

The geometry-optimized radical minima of Figure 6 were calculated with Gaussian 98 on a personal computer[38] or on a University of Illinois, Urbana−Champaign NCSA supercomputer.[39] DFT was preferred over basic Hartree−Fock calculations because reasonably high accuracy was desired, but the molecules proved too large for MP2 calculations. Of the various DFT methods, B3PW91 was selected since it has been shown to be the best three-parameter hybrid method for minima,[40] and the hybrid methods exhibit superior performance as compared to the pure DFT methods for most computational applications. The 6-31G basis set[41] augmented with one set of d diffuse functions[42] and one set of d polarization functions[43] on the heavy atoms (6-31+G*) was used. The nature of the stationary points was verified by frequency calculations.

For the three-dimensional potential energy surface of Figure 5, less expensive UHF/6-31+G* calculations were used as implemented in GAMESS (Version 26, October 2000, from Iowa State University).[44] Spin-restricted open-shell Hartree−Fock was also attempted in the region of the transition state (ROHF/6-31+G*), but while the results were qualitatively similar, the wave function (as one would expect) proved to be unstable near the transition state.

Acknowledgment. We thank Faye L. Stump for the synthesis of compounds **4**, **5**, and **6**. Support from Arizona State University and The Research Corporation is gratefully acknowledged. Some of the electronic structure calculations were performed using NCSA Grants CHE010038N, CHE020011N.

Supporting Information Available: Experimental details of the picosecond and femtosecond transient absorption spectra, including CT complexes studied, excitation and observation wavelengths, and raw experimental data (PDF). This material is available free of charge via the Internet at http://pubs.acs.org.

JA020768E

(38) Frisch, M. J.; Trucks, G. W.; Schlegel, H. B.; Scuseria, G. E.; Robb, M. A.; Cheeseman, J. R.; Zakrzewski, V. G.; Montgomery, J. A., Jr., Stratmann, R. E.; Burant, J. C.; Dapprich, S.; Millam, J. M.; Daniels, A. D.; Kudin, K. N.; Strain, M. C.; Farkas, O.; Tomasi, J.; Barone, V.; Cossi, M.; Cammi, R.; Mennucci, B.; Pomelli, C.; Adamo, C.; Clifford, S.; Ochterski, J.; Petersson, G. A.; Ayala, P. Y.; Cui, Q.; Morokuma, K.; Malick, D. K.; Rabuck, A. D.; Raghavachari, K.; Foresman, J. B.; Cioslowski, J.; Ortiz, J. V.; Baboul, A. G.; Stefanov, B. B.; Liu, G.; Liashenko, A.; Piskorz, P.; Komaromi, I.; Gomperts, R.; Martin, R. L.; Fox, D. J.; Keith, T.; Al-Laham, M. A.; Peng, C. Y.; Nanayakkara, A.; Gonzalez, C.; Challacombe, M.; Gill, P. M. W.; Johnson, B.; Chen, W.; Wong, M. W.; Andres, J. L.; Gonzalez, C.; Head-Gordon, M.; Replogle, E. S.; Pople, J. A. *Gaussian 98*, Rev. A.7; Gaussian, Inc.: Pittsburgh, PA, 1998.

(39) Frisch, M. J.; Trucks, G. W.; Schlegel, H. B.; Scuseria, G. E.; Robb, M. A.; Cheeseman, J. R.; Zakrzewski, V. G.; Montgomery, J. A., Jr., Stratmann, R. E.; Burant, J. C.; Dapprich, S.; Millam, J. M.; Daniels, A. D.; Kudin, K. N.; Strain, M. C.; Farkas, O.; Tomasi, J.; Barone, V.; Cossi, M.; Cammi, R.; Mennucci, B.; Pomelli, C.; Adamo, C.; Clifford, S.; Ochterski, J.; Petersson, G. A.; Ayala, P. Y.; Cui, Q.; Morokuma, K.; Rega, N,; Salvador, P.; Dannenberg, J. J.; Malick, D. K.; Rabuck, A. D.; Raghavachari, K.; Foresman, J. B.; Cioslowski, J.; Ortiz, J. V.; Baboul, A. G.; Stefanov, B. B.; Liu, G.; Liashenko, A.; Piskorz, P.; Komaromi, I.; Gomperts, R.; Martin, R. L.; Fox, D. J.; Keith, T.; Al-Laham, M. A.; Peng, C. Y.; Nanayakkara, A.; Challacombe, M.; Gill, P. M. W.; Johnson, B.; Chen, W.; Wong, M. W.; Andres, J. L.; Gonzalez, C.; Head-Gordon, M.; Replogle, E. S.; Pople, J. A. *Gaussian 98*, Rev. A.11.2; Gaussian, Inc.: Pittsburgh, PA, 2002.

(40) Becke, A. D. *J. Chem. Phys.* **1993**, *98*, 5648.

(41) (a) Ditchfield, R.; Hehre, W. J.; Pople, J. A. *J. Chem. Phys.* **1971**, *54*, 724. (b) Here, W. J.; Ditchfield, R.; Pople, J. A. *J. Chem. Phys.* **1972**, *56*, 2257.

(42) Clark, T.; Chandrasekhar, J.; Spitznagel, G. W.; Schleyer, P. v. R. *J. Comput. Chem.* **1983**, *4*, 294.

(43) (a) Harihan, P. C.; Pople, J. A. *Theor. Chim. Acta* **1973**, *28*, 213. (b) Franci, M. M.; Pietro, W. J.; Hehre, W. J.; Binkley, J. S.; Gordon, M. S.; DeFrees, D. J.; Pople, J. A. *J. Chem. Phys.* **1982**, *77*, 3654.

(44) Schmidt, M. W.; Baldridge, K. K.; Boatz, J. A.; Elbert, S. T.; Gordon, M. S.; Jensen, J. H.; Koseki, S.; Matsunaga, N.; Nguyen, K. A.; Su, S. J.; Windus, T. L.; Dupuis, M.; Montgomery, J. A. *J. Comput. Chem.* **1993**, *14*, 1347.